Available online at www.sciencedirect.com
ScienceDirect
Journal of Computational Physics 227 (2008) 2481–2513
JOURNAL OF COMPUTATIONAL PHYSICS
www.elsevier.com/locate/jcp

Solvers for the high-order Riemann problem for hyperbolic balance laws

C.E. Castro [a,*], E.F. Toro [b]

[a] Geophysics Department of Earth and Environmental Sciences, Munich University, Germany
[b] Laboratory of Applied Mathematics, Department of Civil and Environmental Engineering, University of Trento, Italy

Received 16 November 2006; received in revised form 9 October 2007; accepted 2 November 2007
Available online 22 November 2007

The authors dedicate this paper to P.L. Roe, on occasion of his 70th birthday.

Abstract

We study three methods for solving the Cauchy problem for a system of non-linear hyperbolic balance laws with initial condition consisting of two smooth vectors, with a discontinuity at the origin, a high-order Riemann problem. Two of the methods are new; one of the them results from a re-interpretation of the high-order numerical methods proposed by Harten et al. [A. Harten, B. Engquist, S. Osher, S.R. Chakravarthy, Uniformly high order accuracy essentially non-oscillatory schemes III, J. Comput. Phys. 71 (1987) 231–303] and the other is a modification of the solver in [E.F. Toro, V.A. Titarev, Solution of the generalised Riemann problem for advection-reaction equations, Proc. Roy. Soc. London A 458 (2002) 271–281]. A systematic assessment of all three solvers is carried out and their relative merits are discussed. We also implement the solvers, locally, in the context of high-order finite volume numerical methods of the ADER type, on unstructured meshes. Schemes of up to fifth order of accuracy in space and time for the two-dimensional compressible Euler equations and the shallow water equations with source terms are constructed. Empirically obtained convergence rates are studied systematically and, for the tests considered, these correspond to the theoretically expected orders of accuracy. We also address the question of balance between flux gradients and source terms, for steady flow. We find that the ADER schemes may be termed asymptotically well-balanced, in the sense that the *well-balanced* property is attained as the order of the method increases, and this without introducing any ad-hoc fixes to the schemes or the equations.

Keywords: Hyperbolic equations; Source terms; Classical Riemann problem; High-order Riemann problem; Godunov method; ADER methods; Euler equations; Shallow water equations; Unstructured meshes; Well-balanced schemes

1. Introduction

This paper is concerned with methods to solve the Cauchy problem for general systems of non-linear hyperbolic equations with source terms and initial conditions consisting of two smooth vectors, typically made up of

* Corresponding author. Tel.: +49 89 2180 4138; fax: +49 89 2180 4205.
E-mail addresses: castro@geophysik.uni-muenchen.de (C.E. Castro), toro@ing.unitn.it (E.F. Toro).
URLs: http://www.geophysik.uni-muenchen.de/Members/castro (C.E. Castro), http://www.ing.unitn.it/toro/ (E.F. Toro).

0021-9991/$ - see front matter © 2007 Elsevier Inc. All rights reserved.
doi:10.1016/j.jcp.2007.11.013

polynomials of arbitrary degree, separated by a discontinuity at the origin. This Cauchy problem is a generalization of the *classical Riemann problem*, which we define as the Cauchy problem for a system of homogeneous conservation laws, with initial condition consisting of two *constant* states separated by a discontinuity at the origin. A method of solution for this classical Riemann problem was put forward by Godunov [15], who was the first to use the solution of this problem, locally, to construct his first-order upwind numerical scheme. Today there exists a wide variety of approaches for solving this classical Riemann problem, exactly and approximately. Many of these methods are studied, for example, in [41]. This paper is concerned with the high-order Riemann problem, a generalization of the classical Riemann problem.

The classical Riemann problem can be generalized in a number of ways of which two are the most common: (i) generalization of the equations by adding source terms, for example, and (ii) generalization of the initial conditions, to include piece-wise smooth data. The pioneering work of Liu [27] for hyperbolic systems contained elements of both types of generalizations; Liu used his method to prove global existence of solutions. Later Fok [12] used the Liu solver in a numerical setting using the Random Choice Method. Fok's work was subsequently improved by Glimm and collaborators [14], who incorporated a more accurate solution of the generalized Riemann problem. We remark that in order to apply the solution to the Random Choice Method it is necessary to know the solution in a certain region of space and time. Thus the solution procedure is much more involved than that for use in most Godunov-type methods, for which one only requires the solution at the position of the initial discontinuity, the interface. See the related work of Men'shov [28]. In this paper we are interested in the solution of the generalized Riemann problem at the interface, as a function of time, and this defines a different direction of the research.

Regarding the generalization of the initial conditions in the classical Riemann problem, the simplest case is that in which these consist of two vectors of first degree polynomials (piece-wise linear data) separated by a discontinuity at the origin. This generalization of the classical Riemann problem has been extensively used, for more than three decades, to construct Godunov-type schemes of second order of accuracy. See for example the pioneering work of Ben-Artzi and Falcovitz [1]. In [2] the authors provide a very comprehensive study of this Cauchy problem as well as its use for constructing second-order Godunov-type methods; see also their more recent related works on the subject [3,4]. In the numerical literature this, homogeneous, Cauchy problem with piece-wise linear data has been termed the *generalized Riemann problem*, or GRP. Other related works on the GRP are [29,47,1,48,6,5,28,39–41,2].

The terminology *generalized Riemann problem* has also been used to mean the still more general Cauchy problem with piece-wise smooth initial conditions, typically two vectors of polynomials of arbitrary degree. See for example the works of [24,16,25,26], and references therein. A still more general Riemann-type problem is that in which the governing non-linear equations have source terms and the initial conditions are piece-wise smooth. This Cauchy problem was considered in [44,46], for which a semi-analytical method of solution was proposed; they called this Cauchy problem the *Derivative Riemann Problem*, or DRP and generalizes the following simpler cases: (a) non-linear inhomogeneous equations and piece-wise constant initial conditions; (b) non-linear homogeneous equations and piece-wise linear initial conditions; (c) non-linear homogeneous equations and piece-wise smooth initial conditions.

The method of [44,46] to solve the Derivative Riemann Problem has its origin in a simplified version, first communicated in [39,40], of the GRP method of Ben-Artzi and Falcovitz [1]. The resulting simplified second-order scheme was termed the *Modified GRP* scheme, or *MGRP*, in [40]. The difference between the GRP scheme of Ben-Artzi and Falcovitz and the *MGRP* of Toro is in the way the second term of the asymptotic expansion is calculated. In the *MGRP* (i) one uses the Cauchy–Kowalewski procedure to express time derivatives in terms of space derivatives and (ii) one then solves a (classical) linear Riemann problem for the first-order space derivative of the vector of unknowns, at the origin. An extension of the *MGRP* approach, that involves the solution of linear Riemann problems for the space derivatives, to linear homogeneous system with piece-wise smooth polynomial data was reported in [42]. The solution of these local Cauchy problems were used to construct high-order numerical methods for one, two and three space dimensions, in Cartesian geometries; implementations included schemes of upto 10th order of accuracy in space and time for the one and two-dimensional linear advection equation. The authors in [42] called the resulting high-order numerical methods: ADER (**A**rbitrary Accuracy **DER**ivative Riemann problem).

The method of [44,46] generalizes that of [40,42] and applies to non-linear systems with source terms and piece-wise smooth initial conditions, such as polynomials of arbitrary degree. One begins by first expressing the time-dependent solution at the interface as an asymptotic expansion of order K, as done for example in [25]. The leading term of the expansion is the solution of a classical, usually non-linear, Riemann problem with initial conditions consisting of the limiting values (constant) from either side of the discontinuity. This part is identical to the GPR scheme of Ben-Artzi and Falcovitz [1] and the *MGRP* scheme of Toro [40]. The procedure to determine the higher order terms follows the *MGRP* approach. One first uses the Cauchy–Kowalewski procedure to express time derivatives in terms of functions (or functionals) whose arguments are spatial derivatives of the vector of unknowns. We note that in the presence of source terms, these are included in the Cauchy–Kowalewski procedure. Then the problem is that of determining the arguments of these functionals, spatial derivatives. In order to define the spatial derivatives one first constructs new evolution equations for these and then solves additional, classical, Riemann problems for spatial derivatives of the desired order. The solutions of these classical Riemann problems define all spatial derivatives at the interface and thus the arguments of the functionals are determined. The complete solution is then built up by evaluating the functionals of spatial derivatives and assembling the complete series. In this manner the method of solution of order K boils down to solving 1 classical non-linear Riemann problem for the leading term and K classical linear Riemann problems for spatial derivatives. The described procedure leads to the determination of numerical fluxes, which include the influence of the source terms, if present in the original equations. To fully account for the presence of source terms in a numerical method one requires additionally the evaluation of a volume integral to high order of accuracy, consistent with that for the flux. Analogous methods to those described for the flux are applied to determine the integrand of the volume integral.

Numerical methods of arbitrary order of accuracy can be constructed as a straight generalization of Godunov's first order method, by using the solution of the DRP at the interface. These methods were called ADER methods in [42]. For computed solutions with a (pre-assigned) relatively large error, it is unclear as to whether it is more efficient to use a low order method on a fine mesh or a high-order method on a coarse mesh. However, for computing a solutions with a small (pre-assigned) error it is distinctly more efficient to use high-order methods, and by a huge margin. See the work of Dumbser et al. [10]. Corresponding schemes for non-linear systems based on the DRP solver in [44], were reported in [37,45,38]. Further developments of ADER schemes are reported in [36,32,21,33,22,31,23,9,7,11].

The present paper is motivated by a number of issues. First, it appears necessary to examine more closely the quality of the approximate solutions produced by the existing DRP solver of Toro and Titarev [44], for the case of non-linear systems. In addition, we have recently identified a class of problems for which this DRP solver may experience some difficulties. The problems in question include, locally, a stationary discontinuity, a shock wave or a contact wave, for which the DRP expansion of [44] may be non-unique, giving rise to a non-unique choice of intercell numerical flux. At the level of the first-order scheme the choice is unique due to the Rankine–Hugoniot conditions that ensure the continuity of the flux; that is, the flux is the same whether taken from the left or from the right of the interface. For the high-order schemes the fluxes are different. We also present new DRP solvers and discuss their relative performance, at the local level, as well as a means to provide a numerical flux for high-order methods. The high-order method proposed by Harten, Engquist, Osher and Chakravarthy [17], after a minor modification, may be interpreted in the frame of the ADER methods. That is, we could define an associated derivative Riemann problem with a corresponding method to solve it. We call the resulting method the HEOC solver, which in its re-interpreted version includes source terms. In this paper we also propose a new solver; this is a modification of that of Toro and Titarev [44]. The main feature of this new DRP solver is that the high-order terms are computed by solving linearized classical Riemann problems for the high-order *time derivatives*, directly. This is motivated by the fact that for a linear system, all-order time derivatives obey the original system of PDEs. We prove that for the case of a linear system with constant coefficients all three methods studied here coincide and their solution is identical to the exact solution of the DRP problem. For special cases we also relate the three solvers to the *acoustic approximation* of Ben-Artzi and Falcovitz [2].

A systematic assessment of the methods to solve the DRP for non-linear systems is performed, through a carefully selected suite of test problems. We also implement some of the schemes to construct high-order numerical methods to solve the general initial boundary value problem. The methods are implemented and

assessed for one-dimensional problems and for two-dimensional problems on unstructured meshes. Convergence rates of the schemes for one and two-dimensional test problems are studied. We also address the question of balance between flux gradients and source terms, for steady flow, and the so-called *well-balanced* schemes. We find that the ADER schemes may be termed asymptotically well-balanced, in the sense that the *well-balanced* property is attained as the order of the method increases, and this without introducing any ad-hoc fixes to the schemes or to the formulation of the original equations.

The rest of this paper is organized as follows. In Section 2 we define the mathematical problem and review an existing DRP solver. In Section 3 we present two new DRP solvers. Section 4 deals with the DRP solvers in the context of high-order finite volume methods in one-space dimension. In Section 5 we assess the performance of the local DRP solvers. In Section 6 we implement ADER high order numerical methods for two-dimensional systems on unstructured meshes and for the shallow water equations with source terms. Conclusions are drawn in Section 7.

2. The derivative Riemann problem

Here we first state the mathematical problem and then briefly review an existing semi-analytical method to compute the solution at the interface as a function of time.

2.1. The mathematical problem

In this paper we are interested in methods for solving the high-order Riemann problem

$$\left.\begin{array}{ll} \text{PDEs:} & \partial_t \mathbf{Q} + \partial_x \mathbf{F}(\mathbf{Q}) = \mathbf{S}(\mathbf{Q}), \quad x \in (-\infty, \infty), \quad t > 0, \\ \text{IC:} & \mathbf{Q}(x,0) = \begin{cases} \mathbf{Q}_L(x) & \text{if } x < 0, \\ \mathbf{Q}_R(x) & \text{if } x > 0. \end{cases} \end{array}\right\} \tag{1}$$

This cauchy problem was studied in [44,46] and has been termed by them the *Derivative Riemann Problem*, terminology that we shall adopt here.

The partial differential equations (PDEs), with source terms, are assumed to be a general system of hyperbolic balance laws. The initial condition (IC) consists of two vectors $\mathbf{Q}_L(x)$ and $\mathbf{Q}_R(x)$, the components of which are assumed to be smooth functions of x, with K continuous non-trivial spatial derivatives away from zero. We denote by DRP_{K} the Cauchy problem (1). In the DRP_0 all first and higher-order spatial derivatives of the initial condition away from the origin vanish identically; this case corresponds to the *classical* piece-wise constant data Riemann problem, associated with the first-order Godunov scheme [15]. Similarly, in the DRP_1 all second and higher-order spatial derivatives of the initial condition for the DRP away from the origin vanish identically; this case corresponds to the piece-wise linear data Riemann problem, or the so-called generalized Riemann problem (GRP), associated with a second-order method of the Godunov type [29,47,1,6,5,28,40,2].

Fig. 1 depicts the classical Riemann problem DRP_0 for a typical 3×3 homogeneous non-linear system, for which it is assumed that the left wave is a rarefaction, the right wave is a shock and the middle wave is a contact. The top frame shows the initial condition for a single component q of the vector of unknowns $\mathbf{Q}$. The bottom frame of Fig. 1 depicts the structure of the corresponding solution in the $x - t$ plane; characteristic curves are straight lines. We note however, that the solution of the Riemann problem with piece-wise constant data but with source terms does not have a similarity solution and cannot be represented as in Fig. 1 (bottom frame).

Fig. 2 illustrates the Derivative Riemann Problem DRP_K; the top frame depicts the initial condition for a single component q and consists of two smooth vectors separated by a discontinuity at the origin. The bottom frame of Fig. 2 depicts the corresponding structure of the solution in the $x - t$ plane. Now characteristics are no longer straight lines. Compare Figs. 1 and 2. The aim of this paper is to present methods to find the solution of (1) at the origin $x = 0$ and for $t > 0$, as a function of time and represented by $Q_{LR}(\tau)$ in Fig. 2. Recall that for the classical (homogeneous) Riemann problem the solution is self-similar, it depends on the ratio x/t and is constant at $x = 0$ (the interface) for $t > 0$. In many situations of interest one can find the solution everywhere in the half plane $x \in (-\infty, \infty), t > 0$, although for the purpose of computing a numerical flux, knowing

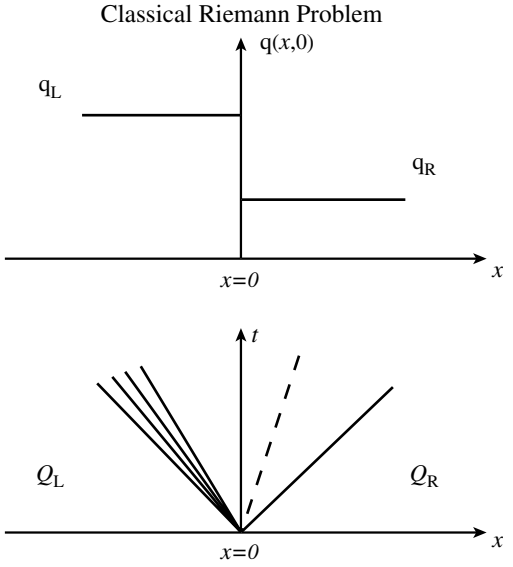

Fig. 1. The classical Riemann problem for a typical 3×3 non-linear homogeneous system. Top frame: initial condition at $t = 0$ for a single component q of the vector of unknowns $\mathbf{Q}$. Bottom frame: structure of the solution in the $x - t$ plane.

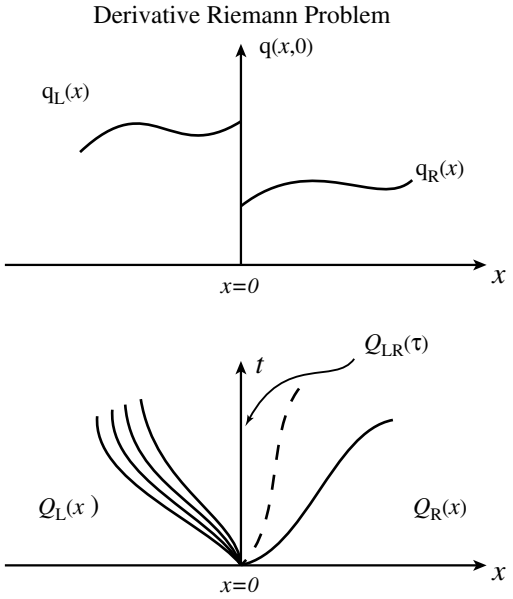

Fig. 2. The Derivative Riemann Problem for a typical 3×3 non-linear system. Top frame: initial condition at $t = 0$ for a single component q of the vector of unknowns $\mathbf{Q}$. Bottom frame: structure of the solution in the $x - t$ plane.

the solution along the interface is sufficient. For the derivative Riemann problem DRP_K, with $K > 0$, finding the solution in the half plane $x \in (-\infty, \infty), t > 0$, is a formidable task that is possible only in special cases. See [28] for the complete solution of the DRP_1 for the Euler equations for ideal gases.

To construct high-order numerical methods of the ADER type [42] it is sufficient to find the solution $\mathbf{Q}_{LR}(\tau)$ at the interface position $x = 0$, as a function of time τ alone. $\mathbf{Q}_{LR}(\tau)$ will provide sufficient information to compute a numerical flux to construct a numerical scheme of $(K + 1)$th order of accuracy in both space and time. The corresponding intercell numerical flux, denoted by $\mathbf{F}_{LR}$, is the time-integral average

$$\mathbf{F}_{LR} = \frac{1}{\Delta t}\int_0^{\Delta t} \mathbf{F}(\mathbf{Q}_{LR}(\tau))\mathrm{d}\tau, \tag{2}$$

where Δt is the time step of the scheme. Numerical methods based on this framework were called ADER methods in [42]. Early versions of the approach were communicated in [39,40].

Note that the conventional case of piece-wise constant data reproduces the classical first-order upwind method of Godunov [15].

2.2. A Known Method of Solution: the Toro–Titarev (TT) solver

Here we briefly review the method proposed by Toro and Titarev [44,46], whereby a semi-analytical solution of the Derivative Riemann Problem (1) is obtained. Their method, as in [1] for second order and in [25] for the general case, first expresses the sought solution $\mathbf{Q}_{LR}(\tau)$ at the interface $x = 0$ as the power series expansion in time

$$\mathbf{Q}_{LR}(\tau) = \mathbf{Q}(0,0_+) + \sum_{k=1}^{K}\left[\partial_t^{(k)}\mathbf{Q}(0,0_+)\right]\frac{\tau^k}{k!}, \tag{3}$$

where

$$\mathbf{Q}(0,0_+) = \lim_{t\to 0_+}\mathbf{Q}(0,t).$$

The solution contains the leading term $\mathbf{Q}(0,0_+)$ and higher-order terms, with coefficients determined by the time derivatives $\partial_t^{(k)}\mathbf{Q}(0,0_+)$. The determination of all terms in the expansion includes the following steps:

Step (I): The leading term. To compute the leading term one solves exactly or approximately the classical Riemann problem

$$\left.\begin{array}{ll} \text{PDEs:} & \partial_t\mathbf{Q} + \partial_x\mathbf{F}(\mathbf{Q}) = \mathbf{0}, \\ \text{ICs:} & \mathbf{Q}(x,0) = \begin{cases} \mathbf{Q}_L(0_-) & \text{if } x < 0, \\ \mathbf{Q}_R(0_+) & \text{if } x > 0, \end{cases} \end{array}\right\} \tag{4}$$

with

$$\mathbf{Q}_L(0_-) = \lim_{x\to 0_-}\mathbf{Q}_L(x), \quad \mathbf{Q}_R(0_+) = \lim_{x\to 0_+}\mathbf{Q}_R(x). \tag{5}$$

The similarity solution of (4) is denoted by $\mathbf{D}^{(0)}(x/t)$ and the leading term in (3) is

$$\mathbf{Q}(0,0_+) = \mathbf{D}^{(0)}(0). \tag{6}$$

Step (II): Higher order terms. There are three sub-steps here.

(1) **Time derivatives in terms of spatial derivatives:** Use the Cauchy–Kowalewski procedure to express time derivatives in (3) in terms of functionals of space derivatives

$$\partial_t^{(k)}\mathbf{Q}(x,t) = \mathbf{G}^{(k)}(\partial_x^{(0)}\mathbf{Q}, \partial_x^{(1)}\mathbf{Q}, \ldots, \partial_x^{(k)}\mathbf{Q}). \tag{7}$$

The source term $\mathbf{S}(\mathbf{Q})$ in (1) is included in the arguments of $\mathbf{G}^{(k)}$. The problem now is that of determining the arguments of $\mathbf{G}^{(k)}$, namely the spatial derivatives at the interface. An illustration of the Cauchy–Kowalewski procedure is given in Section 2.3.

(2) **Evolution equations for derivatives:** Construct evolution equations for spatial derivatives

$$\partial_t(\partial_x^{(k)}\mathbf{Q}(x,t)) + \mathbf{A}(\mathbf{Q})\partial_x(\partial_x^{(k)}\mathbf{Q}(x,t)) = \mathbf{H}^{(k)}, \tag{8}$$

where $\mathbf{A}(\mathbf{Q})$ is the Jacobian matrix of the PDEs in (1).

(3) **Riemann problems for spatial derivatives:** Given that the above equations are too complicated Toro and Titarev [44,46] assumed equations (8) to be linear with constant coefficient matrix $\mathbf{A}_{LR}^{(0)} = \mathbf{A}(\mathbf{Q}(0,0_+))$ and homogeneous. We remark that one could also arrive at the same result

assuming from the outset, only in this step, that the governing equations are linear with constant coefficients. See Section 3.3.1.Then to determine the spatial derivatives at the interface one poses classical, homogeneous linearized Riemann problems for spatial derivatives as follows

$$\left.\begin{array}{ll}\text{PDEs:} & \partial_t(\partial_x^{(k)}\mathbf{Q}(x,t)) + \mathbf{A}_{LR}^{(0)}\partial_x(\partial_x^{(k)}\mathbf{Q}(x,t)) = \mathbf{0}, \\ \text{ICs:} & \partial_x^{(k)}\mathbf{Q}(x,0) = \begin{cases} \partial_x^{(k)}\mathbf{Q}_L(0_-) & \text{if } x<0, \\ \partial_x^{(k)}\mathbf{Q}_R(0_+) & \text{if } x>0. \end{cases}\end{array}\right\} \tag{9}$$

Solve these Riemann problems to obtain similarity solutions $\mathbf{D}^{(k)}(x/t)$ and set

$$\partial_x^{(k)}\mathbf{Q}(0,0_+) = \mathbf{D}^{(k)}(0). \tag{10}$$

Step (III): The solution. Form the solution as the power series expansion:

$$\mathbf{Q}_{LR}(\tau) = \mathbf{C_0} + \mathbf{C_1}\tau + \mathbf{C_2}\tau^2 + \cdots + \mathbf{C_K}\tau^K, \tag{11}$$

with $\mathbf{C}_0$ as in (6) and

$$\mathbf{C}_k \equiv \frac{\partial_t^{(k)}\mathbf{Q}(0,0_+)}{k!} = \frac{\mathbf{G}^{(k)}(\mathbf{D}^{(0)}(0),\mathbf{D}^{(1)}(0),\ldots,\mathbf{D}^{(k)}(0))}{k!}, \tag{12}$$

for $k = 1,\ldots,K$.

This solution technique for the Derivative Riemann Problem DRP_K reduces the problem to that of solving $K+1$ classical homogeneous Riemann problems, one (generally non-linear) Riemann problem to compute the leading term and K linearized Riemann problems to determine the higher order terms.

The leading term requires the availability of a *Riemann solver*, exact or approximate. The K linearized Riemann problems (9) for most well-known systems associated with the higher order terms can be solved analytically and no choice of a *Riemann solver* is necessary. Moreover, all of these linearized problems have the same eigenstructure, as the coefficient matrix is the same for all Riemann problems for derivatives.

In principle, the technique can be applied to calculate the early-time solution of advection-reaction equations with piece-wise smooth initial conditions. One can set up a derivative Riemann problem at any desired position, taking care that at each point $x = x_d$ of discontinuity in the initial condition one sets a corresponding derivative Riemann problem centred at x_d. The solution at each point x_d, for a small time τ, can be used to check the results of numerical schemes.

2.3. Illustration of the Cauchy–Kowalewski procedure

Here we illustrate the application of the Cauchy–Kowalewski procedure to express time derivatives in terms of spatial derivatives, by applying it to the non-linear wave equation with source term

$$\partial_t q(x,t) + \partial_x f(q(x,t)) = s(q(x,t)). \tag{13}$$

We assume $q(x,t)$ to be continuous and differentiable up to order K. From (13) it is immediate that the first-order time derivative is

$$\partial_t q(x,t) = -\lambda(q)\partial_x q(x,t) + s(q) \equiv g^{(1)}(\partial_x^{(0)}q, \partial_x^{(1)}q), \tag{14}$$

where $\lambda(q) = f'(q)$ and the functional $g^{(1)}$ is

$$g^{(1)}(\partial_x^{(0)}q, \partial_x^{(1)}q) = -f'(\partial_x^{(0)}q) \times \partial_x^{(1)}q + s(\partial_x^{(0)}q), \quad \partial_x^{(0)}q = q. \tag{15}$$

In the same way, the second-order time derivative is

$$\begin{aligned}\partial_t^{(2)}q(x,t) &= (f'(q))^2\partial_x^{(2)}q(x,t) + 2f'(q)f''(q)(\partial_x^{(1)}q(x,t))^2 - \partial_x^{(1)}q(x,t)(f''(q)s(q) + 2f'(q)s'(q)) + s'(q)s(q)s \\ &\equiv g^{(2)}(\partial_x^{(0)}q, \partial_x^{(1)}q, \partial_x^{(2)}q).\end{aligned} \tag{16}$$

In this case the functional $g^{(2)}$ is more complicated; its arguments are spatial derivatives of $q(x,t)$. In general, the *kth* order time derivative is written as a functional depending on the space derivatives up to order k

$$\partial_t^{(k)} q(x,t) = g^{(k)}(\partial_x^{(0)} q, \partial_x^{(1)} q, \ldots, \partial_x^{(k-1)} q, \partial_x^{(k)} q), \tag{17}$$

for $k = 1 \ldots K$. In practice, for the more general case of non-linear systems we use symbolic manipulators to compute the functional $\mathbf{G}^{(k)}$ in (7) and (17).

3. Other methods of solution

Here we study two alternative methods for solving the DRP (1). The first results from a re-interpretation of the high-order numerical method first proposed by Harten et al. [17]. Consequently we call this derivative Riemann problem solver, the Harten–Engquist–Osher–Chakravarthy (HEOC) solver. The second method we study results from a modification of both the Toro–Titarev solver [44] of Section 2.2 and the HEOC solver.

3.1. The Harten–Engquist–Osher–Chakravarthy (HEOC) solver

Here we re-interpret the method proposed by Harten, Engquist, Osher and Chakravarthy [17] to compute numerical fluxes for their high-order methods, as a technique to provide an approximate solution to the derivative Riemann problem (1) at the interface $x = 0$, as a function of time. They proposed power series expansions in space and time for the solution in each control volume, or cell. There followed the application of the Cauchy–Kowalewski method to convert all time derivatives in the expansions to space derivatives, which in turn could be computed on the initial data.

In our re-interpretation we include source terms in the equations and consider power series expansions in time on each side of the interface defined as follows:

$$\widetilde{\mathbf{Q}}_L(\tau) = \mathbf{Q}_L(0_-) + \sum_{k=1}^{K} [\partial_t^{(k)} \mathbf{Q}(0_-, 0)] \frac{\tau^k}{k!} \tag{18}$$

and

$$\widetilde{\mathbf{Q}}_R(\tau) = \mathbf{Q}_R(0_+) + \sum_{k=1}^{K} [\partial_t^{(k)} \mathbf{Q}(0_+, 0)] \frac{\tau^k}{k!}, \tag{19}$$

with

$$\mathbf{Q}(0_-, 0) = \lim_{x \to 0_-} \mathbf{Q}(x, 0) \equiv \mathbf{Q}_L(0_-) \tag{20}$$

and

$$\mathbf{Q}(0_+, 0) = \lim_{x \to 0_+} \mathbf{Q}(x, 0) \equiv \mathbf{Q}_R(0_+). \tag{21}$$

The Cauchy–Kowalewski procedure allows us to use the PDEs in (1) to express all time derivatives in (18) and (19) as functions (or functionals) of space derivatives and of the source terms $\mathbf{S}(\mathbf{Q})$, namely

$$\partial_t^{(k)} \mathbf{Q}(x,t) = \mathbf{G}^{(k)}(\partial_x^{(0)} \mathbf{Q}, \partial_x^{(1)} \mathbf{Q}, \ldots, \partial_x^{(k)} \mathbf{Q}). \tag{22}$$

See the illustration of the Cauchy–Kowalewski procedure in Section 2.3. These expressions are well defined to the left and right of the interface, given that the initial conditions in (1) are assumed to be smooth away from 0. We can also define the limiting values from left and right, at $t = 0$, of the spatial derivatives of the initial conditions, namely

$$\mathbf{Q}_L^{(k)}(0_-) \equiv \lim_{x \to 0_-} \frac{\mathrm{d}^k}{\mathrm{d}x^k} \mathbf{Q}_L(x), \tag{23}$$

$$\mathbf{Q}_R^{(k)}(0_+) \equiv \lim_{x \to 0_+} \frac{\mathrm{d}^k}{\mathrm{d}x^k} \mathbf{Q}_R(x). \tag{24}$$

Thus we have

$$\partial_t^{(k)}\mathbf{Q}(0_-,0) = \mathbf{G}^{(k)}(\mathbf{Q}_L^{(0)}(0_-), \mathbf{Q}_L^{(1)}(0_-), \ldots, \mathbf{Q}_L^{(k)}(0_-)) \tag{25}$$

and

$$\partial_t^{(k)}\mathbf{Q}(0_+,0) = \mathbf{G}^{(k)}(\mathbf{Q}_R^{(0)}(0_+), \mathbf{Q}_R^{(1)}(0_+), \ldots, \mathbf{Q}_R^{(k)}(0_+)). \tag{26}$$

We define the solution of the DRP (1) at the interface $x = 0$, at time $t = \tau$ as

$$\mathbf{Q}_{LR}(\tau) = \mathbf{D}(\tau, 0), \tag{27}$$

where now $\mathbf{D}(\tau, x/(t-\tau))$ is the similarity solution of the classical, homogeneous Riemann problem

$$\left.\begin{array}{ll} \text{PDEs:} & \partial_t\mathbf{Q} + \partial_x\mathbf{F}(\mathbf{Q}) = \mathbf{0}, \\ \text{ICs:} & \mathbf{Q}(x,0) = \begin{cases} \widetilde{\mathbf{Q}}_L(\tau) & \text{if } x < 0, \\ \widetilde{\mathbf{Q}}_R(\tau) & \text{if } x > 0. \end{cases} \end{array}\right\} \tag{28}$$

Note that here $\mathbf{D}(\tau, x/(t-\tau))$ depends on the parameter τ. We call this re-interpretation of the method proposed by Harten et al. [17] as a derivative Riemann solver, the Harten–Engquist–Osher–Chakravarthy (HEOC) solver.

Fig. 3 gives an interpretation of the HEOC solution method for the DRP (1). At time $t = 0$ one performs a Taylor series expansion in time on the limiting values of the data left and right of the interface (circles). Upon the application of the Cauchy–Kowalewski method one evolves the data in time on each side of the interface, see (18) and (19), to yield time-evolved states $\widetilde{\mathbf{Q}}_L(\tau)$ and $\widetilde{\mathbf{Q}}_R(\tau)$, at any chosen time $t = \tau$ (rhombuses in Fig. 3). These (constant) states at $t = \tau$ form the initial conditions for a classical Riemann problem, as depicted on the top part of Fig. 3 by the self-similar wave pattern. The sought solution is that given by (27), which is constant along the t-axis associated with the self-similar wave pattern. As the method applies to any time τ one has a time-dependent solution at the interface.

We remark that, just as in the Toro–Titarev solver [44] reviewed in Section 2.2, the HEOC solution method as presented here applies to in-homogeneous non-linear hyperbolic balance laws. The influence of the source term enters via the Cauchy–Kowalewski procedure, in which the source terms enter the coefficients in (18), (19) via (25), (26). But note that at no point in the method it becomes necessary to solve Riemann problems, explicitly accounting for the influence of the source terms.

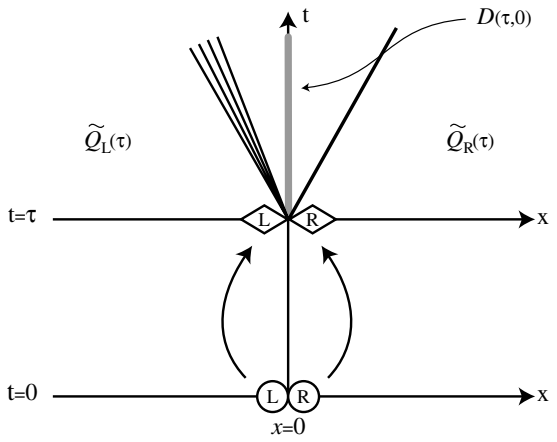

Fig. 3. Illustration of the HEOC Derivative Riemann Problem solver. The limiting values of the initial data from left and right (circles) are time evolved separately to any time τ (rhombuses). The desired solution results from solving the classical Riemann problem with these evolved states as data.

3.2. The Castro–Toro solver

Another method of solution for the DRP (1) results from a modification of both the Harten et al. (HEOC) and the Toro–Titarev (TT) solvers. The sought solution at the interface is again expressed as in (3), with the leading term computed as in (6). This part is identical to the TT solver. To compute the higher order terms we solve *time-derivative* Riemann problems, that is, for any index $k > 0$ we compute $\partial_t^{(k)}\mathbf{Q}(0_-,0)$ and $\partial_t^{(k)}\mathbf{Q}(0_+,0)$ as in (25) (left) and (26) (right). To find $\partial_t^{(k)}\mathbf{Q}(0,0_+)$ right at the interface we solve the classical linearized homogeneous Riemann problem

$$\left.\begin{array}{ll} \text{PDEs}: & \partial_t(\partial_t^{(k)}\mathbf{Q}(x,t)) + \mathbf{A}_{LR}^{(0)}\partial_x(\partial_t^{(k)}\mathbf{Q}(x,t)) = \mathbf{0}, \\ \text{ICs}: & \partial_t^{(k)}\mathbf{Q}(x,0) = \begin{cases} \partial_t^{(k)}\mathbf{Q}(0_-,0) & \text{if } x<0, \\ \partial_t^{(k)}\mathbf{Q}(0_+,0) & \text{if } x>0. \end{cases} \end{array}\right\} \tag{29}$$

The similarity solution is denoted by $\mathbf{T}^{(k)}(x/t)$ and the sought value is

$$\partial_t^{(k)}\mathbf{Q}(0,0_+) = \mathbf{T}^{(k)}(0). \tag{30}$$

The final solution has the form (11) with $\mathbf{C}_0$ as in (6) and

$$\mathbf{C}_k \equiv \frac{\partial_t^{(k)}\mathbf{Q}(0,0_+)}{k!} = \frac{\mathbf{T}^{(k)}(0)}{k!}, \tag{31}$$

for $k = 1,\ldots,K$.

Note the analogy between (9) and (29). Both are motivated by the fact that for a linear homogeneous system with constant coefficient matrix, all temporal and spatial partial derivatives of the vector of unknowns, if defined, obey the original system.

3.3. Special cases

In this section we consider two special DRP problems and compare analytically the various solvers studied in this paper.

3.3.1. Linear systems

Definition. The model DRP problem 1. We define as the model DRP problem 1 the following Cauchy problem

$$\left.\begin{array}{l} \partial_t\mathbf{Q} + \mathbf{A}\partial_x\mathbf{Q} = \mathbf{0}, \quad x\in(-\infty,\infty), \quad t>0, \\ \mathbf{Q}(x,0) \equiv \mathbf{Q}^{(0)}(x) = \begin{cases} \mathbf{P}_L(x) & \text{if } x<0, \\ \mathbf{P}_R(x) & \text{if } x>0, \end{cases} \end{array}\right\} \tag{32}$$

where $\mathbf{Q} = [q_1, q_1, \ldots, q_m]^{\mathrm{T}}$ is the vector of m unknowns; $\mathbf{A}$ is a constant coefficient matrix with m real eigenvalues $\lambda_1 < \lambda_2 < \cdots < \lambda_m$; $\mathbf{R}_1, \mathbf{R}_2, \ldots, \mathbf{R}_m$ are the corresponding linearly independent right eigenvectors so that the matrix of eigenvectors is $\mathbf{R} = [\mathbf{R}_1|\mathbf{R}_2|\cdots|\mathbf{R}_m]$; the functions (vectors) $\mathbf{P}_L(x), \mathbf{P}_R(x)$ are assumed to be polynomials of degree at most K.

Lemma. *The model DRP problem* 1 *defined by* (32) *has exact solution at the interface*

$$\left.\begin{array}{l} \mathbf{Q}(0,\tau) = \displaystyle\sum_{i=1}^{I} c_{R,i}(0)\mathbf{R}_i + \sum_{i=I+1}^{m} c_{L,i}(0)\mathbf{R}_i \\ \qquad + \displaystyle\sum_{k=1}^{K}(-\mathbf{A})^k\left[\sum_{i=1}^{I} c_{R,i}^{(k)}(0)\mathbf{R}_i + \sum_{i=I+1}^{m} c_{L,i}^{(k)}(0)\mathbf{R}_i\right]\frac{\tau^k}{k!} \end{array}\right\} \tag{33}$$

where $\mathbf{W}(x,t) = \mathbf{R}^{-1}\mathbf{Q}(x,t)$ *is the vector of characteristic variables, with*

$$\mathbf{W}(x,0) \equiv \mathbf{W}^{(0)}(x) = \mathbf{R}^{-1}\mathbf{Q}(x,0) = \begin{cases} \mathbf{C}_L(x) \equiv \mathbf{R}^{-1}\mathbf{P}_L(x) & \text{if } x < 0, \\ \mathbf{C}_R(x) \equiv \mathbf{R}^{-1}\mathbf{P}_R(x) & \text{if } x > 0, \end{cases} \tag{34}$$

where the components of $\mathbf{W}^{(0)}(x)$ *are*

$$w_i^{(0)}(x) = \begin{cases} c_{L,i}(x) & \text{if } x < 0, \\ c_{R,i}(x) & \text{if } x > 0 \end{cases} \tag{35}$$

and I *is an integer such that*

$$0 \leqslant I \leqslant m; \quad \lambda_i \leqslant 0 \quad \text{if } i \leqslant I; \quad \lambda_i > 0 \quad \text{if } i > I. \tag{36}$$

Proof. The exact solution of (32) is

$$\mathbf{Q}(x,t) = \sum_{i=1}^{m} w_i^{(0)}(x - \lambda_i t)\mathbf{R}_i. \tag{37}$$

Then from (35), at $x = 0$, we have

$$\mathbf{Q}(0,\tau) = \sum_{i=1}^{I} c_{R,i}(-\lambda_i\tau)\mathbf{R}_i + \sum_{i=I+1}^{m} c_{L,i}(-\lambda_i\tau)\mathbf{R}_i. \tag{38}$$

Taylor expanding in (38) about 0 and using the relation

$$(-\lambda_i)^k\mathbf{R}_i = (-\mathbf{A})^k\mathbf{R}_i \tag{39}$$

we obtain

$$c_{M,i}(-\lambda_i\tau)\mathbf{I} = c_{M,i}(0)\mathbf{I} + \sum_{k=1}^{K}(-\mathbf{A})^k c_{M,i}^{(k)}(0)\frac{\tau^k}{k!}; \quad M = L, R, \tag{40}$$

where $\mathbf{I}$ is the identity matrix. Substituting (40) into (38) gives the sough result (33) and the lemma is proved. □

Proposition. *The solution of the model DRP problem* 1 *given by* (32) *using* (*a*) *the Toro–Titarev method*, (*b*) *the Castro–Toro method and* (*c*) *the Harten–Engquist–Osher–Crakravarthy method is exact.*

Proof. Here we prove the proposition only for the Toro–Titarev method, which first expresses the solution at $x = 0$ via the power series expansion

$$\mathbf{Q}_{LR}(\tau) = \mathbf{Q}(0,0_+) + \sum_{k=1}^{K}[\partial_t^{(k)}\mathbf{Q}(0,0_+)]\frac{\tau^k}{k!}. \tag{41}$$

The leading term $\mathbf{Q}(0,0_+)$ is obtained from solving the classical (linear) Riemann problem

$$\left.\begin{aligned} &\partial_t\mathbf{Q} + \mathbf{A}\partial_x\mathbf{Q} = \mathbf{0}, \quad x \in (-\infty,\infty), \quad t > 0, \\ &\mathbf{Q}(x,0) \equiv \mathbf{Q}^{(0)}(x) = \begin{cases} \mathbf{P}_L(0) & \text{if } x < 0, \\ \mathbf{P}_R(0) & \text{if } x > 0, \end{cases} \end{aligned}\right\} \tag{42}$$

whose exact solution is

$$\mathbf{Q}(0,0_+) = \sum_{i=1}^{I} c_{R,i}(0)\mathbf{R}_i + \sum_{i=I+1}^{m} c_{L,i}(0)\mathbf{R}_i, \tag{43}$$

where $c_{L,i}(0)$ and $c_{R,i}(0)$ are respectively the components of $\mathbf{C}_L(x)$ and $\mathbf{C}_R(x)$ in (34).

The high-order terms in (41) require the determination of the coefficients $\partial_t^{(k)}\mathbf{Q}(0,0_+)$. Application of the Cauchy–Kowalewski procedure to the system in (32) gives

$$\partial_t^{(k)}\mathbf{Q}(x,t) = (-\mathbf{A})^k \partial_x^{(k)}\mathbf{Q}(x,t); \quad k = 1,\ldots,K. \tag{44}$$

Note also that

$$\partial_t(\partial_x^{(k)}\mathbf{Q}) + \mathbf{A}\partial_x(\partial_x^{(k)}\mathbf{Q}) = \mathbf{0}, \quad k = 1,\ldots,K \tag{45}$$

and

$$\partial_x^{(k)}\mathbf{Q}(x,0) = \begin{cases} \mathbf{P}_L^{(k)}(0) & \text{if } x < 0, \\ \mathbf{P}_R^{(k)}(0) & \text{if } x > 0. \end{cases} \tag{46}$$

The solution of the classical Riemann problem for derivatives (45) and (46) is

$$\partial_x^{(k)}\mathbf{Q}(0,0_+) = \sum_{i=1}^{I} c_{R,i}^{(k)}(0)\mathbf{R}_i + \sum_{i=I+1}^{m} c_{L,i}^{(k)}(0)\mathbf{R}_i, \tag{47}$$

where now the characteristic variables of the problem are

$$\partial_x^{(k)}\mathbf{W}(x,t) = \mathbf{R}^{-1}\partial_x^{(k)}\mathbf{Q}(x,t)$$

with

$$\partial_x^{(k)}\mathbf{W}(x,0) = \mathbf{R}^{-1}\ \partial_x^{(k)}\mathbf{Q}(x,0) = \begin{cases} \mathbf{C}_L^{(k)}(x) \equiv \mathbf{R}^{-1}\ \mathbf{P}_L^{(k)}(x) & \text{if } x < 0, \\ \mathbf{C}_R^{(k)}(x) \equiv \mathbf{R}^{-1}\ \mathbf{P}_R^{(k)}(x) & \text{if } x > 0. \end{cases} \tag{48}$$

Use of (43), (44) and (47) gives the sought solution and the proposition is thus proved. □

Remark

- The proof for the other two methods is similar and is thus omitted.
- For the case in which the polynomials $\mathbf{P}_L(x)$ and $\mathbf{P}_R(x)$ are of first degree, the GRP method of Ben-Artzi and Falcovitz [2] also reproduces the exact solution.
- If the data states $\mathbf{P}_L(x), \mathbf{P}_R(x)$ in (32) are arbitrary but smooth functions, then the proposed methods TT, HEOC and CT are not exact, due to the truncation of the series expansion (41).

3.3.2. Non-linear systems: the acoustic approximation

Definition. The model DRP problem 2. We define as the model DRP problem 2 the following Cauchy problem

$$\left.\begin{array}{ll} \text{PDEs}: & \partial_t\mathbf{Q} + \partial_x\mathbf{F}(\mathbf{Q}) = \mathbf{0}, \quad x \in (-\infty,\infty), \quad t > 0, \\ \text{IC}: & \mathbf{Q}(x,0) = \begin{cases} \mathbf{P}_L(x) \equiv \widehat{\mathbf{Q}} + x\mathbf{Q}'_L & \text{if } x < 0, \\ \mathbf{P}_R(x) \equiv \widehat{\mathbf{Q}} + x\mathbf{Q}'_R & \text{if } x > 0. \end{cases} \end{array}\right\} \tag{49}$$

This problem considers a nonlinear system of hyperbolic conservation laws but with very special initial condition, namely, the vector of unknowns is continuous at the interface and the data polynomials $\mathbf{P}_L(x)$ and $\mathbf{P}_R(x)$ are of first degree; there is only a discontinuity in the first spatial derivative of the vector of unknowns at the initial time. Ben-Artzi and Falcovitz [2] considered this problem for the Euler equations and solved it by a method called the *acoustic approximation*.

Proposition. *The solution of the model DRP problem* 2 *given by* (49) *obtained with the solvers* (*a*) *Toro–Titarev*, (*b*) *Castro–Toro and* (*c*) *Ben-Artzi and Falcovitz are identical.*

Proof. All three solvers express the solution at the interface via the expansion

$$\mathbf{Q}_{LR}(\tau) = \mathbf{Q}(0,0_+) + \tau\partial_t\mathbf{Q}(0,0_+). \tag{50}$$

The leading term for all three solvers is obviously $\mathbf{Q}(0,0_+) = \widehat{\mathbf{Q}}$. Next we show that the second term containing the time derivative $\partial_t\mathbf{Q}(0,0_+)$ is also identical. We give the details of the proof only for two of the three solvers. In the Toro–Titarev solver one first applies the Cauchy–Kowalewski procedure to express, via the system in (49), the time derivatives in terms of the spatial derivatives, namely

$$\partial_t\mathbf{Q}(x,t) = -\widehat{\mathbf{A}}\partial_x\mathbf{Q}(x,t), \quad \widehat{\mathbf{A}} = \mathbf{A}(\widehat{\mathbf{Q}}), \tag{51}$$

with $\mathbf{A}(\mathbf{Q})$ the Jacobian matrix of the system in (49). Now the problem is reduced to solving for the spatial derivatives at the interface. This is accomplished by solving exactly the following linear Riemann problem

$$\left.\begin{aligned} &\text{PDEs:} \quad \partial_t(\partial_x\mathbf{Q}(x,t)) + \widehat{\mathbf{A}}\partial_x(\partial_x\mathbf{Q}(x,t)) = \mathbf{0}, \\ &\text{ICs:} \quad \partial_x\mathbf{Q}(x,0) = \begin{cases} \mathbf{Q}'_L & \text{if } x < 0, \\ \mathbf{Q}'_R & \text{if } x > 0. \end{cases} \end{aligned}\right\} \tag{52}$$

The exact solution of this linear Riemann problem is given by

$$\partial_x\mathbf{Q}(0,0_+) = \mathbf{Q}'_L + \sum_{\lambda_i \leqslant 0} \alpha_i\mathbf{R}_i, \tag{53}$$

where λ_i and $\mathbf{R}_i$ are respectively the eigenvalues and right eigenvectors of $\widehat{\mathbf{A}}$; α_i are the wave strengths obtained from the solution of the following algebraic linear system

$$\mathbf{\Delta} \equiv \mathbf{Q}'_R - \mathbf{Q}'_L = \sum_{i=1}^{m} \alpha_i\mathbf{R}_i. \tag{54}$$

The final solution is

$$\mathbf{Q}(0,\tau) = \widehat{\mathbf{Q}} - \tau\widehat{\mathbf{A}}\left[\mathbf{Q}'_L + \sum_{\lambda_i \leqslant 0} \alpha_i\mathbf{R}_i\right]. \tag{55}$$

In the Castro–Toro solver one finds the time derivative vector $\partial_t\mathbf{Q}(0,0_+)$ at the interface by directly solving the following linear Riemann problem for time derivatives

$$\left.\begin{aligned} &\text{PDEs:} \quad \partial_t(\partial_t\mathbf{Q}(x,t)) + \widehat{\mathbf{A}}\partial_x(\partial_t\mathbf{Q}(x,t)) = \mathbf{0}, \\ &\text{ICs:} \quad \partial_t\mathbf{Q}(x,0) = \begin{cases} \partial_t\mathbf{Q}(0_-,0) = -\widehat{\mathbf{A}}\mathbf{Q}'_L & \text{if } x < 0, \\ \partial_t\mathbf{Q}(0_+,0) = -\widehat{\mathbf{A}}\mathbf{Q}'_R & \text{if } x > 0. \end{cases} \end{aligned}\right\} \tag{56}$$

The initial conditions in (56) are obtained by applying the Cauchy–Kowalewski procedure on both sides of the interface. The exact solution of this linear Riemann problem is

$$\partial_t\mathbf{Q}(0,0_+) = (\partial_t\mathbf{Q})_L + \sum_{\lambda_i \leqslant 0} \tilde{\alpha}_i\mathbf{R}_i, \tag{57}$$

where $\tilde{\alpha}_i$ are the wave strengths obtained from the solution of the algebraic linear system

$$\widetilde{\mathbf{\Delta}} \equiv \widehat{\mathbf{A}}(\mathbf{Q}'_R - \mathbf{Q}'_L) = \sum_{i=1}^{m} \tilde{\alpha}_i\mathbf{R}_i. \tag{58}$$

We note that $\widetilde{\mathbf{\Delta}} = -\widehat{\mathbf{A}}\mathbf{\Delta}$ and $\tilde{\alpha}_i = -\alpha_i\lambda_i$. Manipulations of (57) and using (53) give

$$\left.\begin{aligned} \partial_t\mathbf{Q}(0,0_+) &= -\widehat{\mathbf{A}}\mathbf{Q}'_L - \sum_{\lambda_i \leqslant 0} \alpha_i\lambda_i\mathbf{R}_i, \\ &= -\widehat{\mathbf{A}}\mathbf{Q}'_L - \widehat{\mathbf{A}}\sum_{\lambda_i \leqslant 0} \alpha_i\mathbf{R}_i, \\ &= -\widehat{\mathbf{A}}\partial_x\mathbf{Q}(0,0_+). \end{aligned}\right\} \tag{59}$$

From (55) and (59) we conclude that the Toro–Titarev and the Castro–Toro solvers give identical solutions to the model problem (49). □

Remark. The solution of the model problem (49) using GRP solver of Ben-Artzi and Falcovitz [1] is identical to those of the previous two solvers. The proof is omitted.

4. High-order numerical schemes

The DRP solvers studied in this paper can be used to construct Godunov-type schemes of arbitrary order of accuracy. Here we consider these schemes in the framework of the finite volume method.

4.1. Finite volume schemes

The finite volume approach for a non-linear system of $m \times m$ hyperbolic equations with source terms

$$\partial_t \mathbf{Q} + \partial_x \mathbf{F}(\mathbf{Q}) = \mathbf{S}(\mathbf{Q}) \tag{60}$$

reads

$$\mathbf{Q}_i^{n+1} = \mathbf{Q}_i^n - \frac{\Delta t}{\Delta x}\left[\mathbf{F}_{i+\frac{1}{2}} - \mathbf{F}_{i-\frac{1}{2}}\right] + \Delta t \mathbf{S}_i, \tag{61}$$

where $\mathbf{Q}_i^n$ is an approximation to the spatial-integral average

$$\mathbf{Q}_i^n = \frac{1}{\Delta x}\int_{x_{i-\frac{1}{2}}}^{x_{i+\frac{1}{2}}} \mathbf{Q}(x, t^n)\mathrm{d}x \tag{62}$$

in the cell $\left[x_{i-\frac{1}{2}}, x_{i+\frac{1}{2}}\right]$. $\mathbf{F}_{i+\frac{1}{2}}$ is the numerical flux, which is an approximation to the time-integral average (2), and $\mathbf{S}_i$ is the numerical source, which is an approximation to a volume integral. The numerical scheme is completely defined once expressions for $\mathbf{F}_{i+\frac{1}{2}}$ and $\mathbf{S}_i$ are provided.

In the ADER method the numerical flux $\mathbf{F}_{i+\frac{1}{2}}$ is computed by solving the Derivative Riemann Problem

$$\left.\begin{array}{ll} \text{PDEs:} & \partial_t \mathbf{Q} + \partial_x \mathbf{F}(\mathbf{Q}) = \mathbf{S}(\mathbf{Q}), \\ \text{IC:} & \mathbf{Q}(x,0) = \begin{cases} \mathbf{P}_i(x) & \text{if } x < 0, \\ \mathbf{P}_{i+1}(x) & \text{if } x > 0, \end{cases} \end{array}\right\} \tag{63}$$

and then computing the time average as in (2). Here $\mathbf{P}_i(x)$ is a vector defined in cell $\left[x_{i-\frac{1}{2}}, x_{i+\frac{1}{2}}\right]$ whose components are reconstructed polynomials of an appropriate degree; likewise $\mathbf{P}_{i+1}(x)$. In principle, any reconstruction procedure can be used but in practice the non-linear ENO and WENO reconstruction procedures are recommended [18,35,34]. The DRP (63) can be solved using any of the methods studied in this paper.

In the ADER approach the numerical source $\mathbf{S}_i$ results from a high-order approximation to the volume-integral average

$$\mathbf{S}_i = \frac{1}{\Delta t}\frac{1}{\Delta x}\int_0^{\Delta t}\int_{x_{i-\frac{1}{2}}}^{x_{i+\frac{1}{2}}} \mathbf{S}(\mathbf{Q}_i(x,t))\mathrm{d}x\,\mathrm{d}t, \tag{64}$$

still denoted by $\mathbf{S}_i$, where $\mathbf{Q}_i(x,t)$ is a high-order approximation to the solution of (60) inside the control volume, obtained as follows. At any numerical integration point $x_d \in \left[x_{i-\frac{1}{2}}, x_{i+\frac{1}{2}}\right]$ the solution $\mathbf{Q}(x_d, \tau)$, as a function of time, is computed using the Cauchy–Kowalewski method,

$$\mathbf{Q}(x_d, \tau) = \mathbf{Q}(x_d, 0) + \sum_{k=1}^{K}[\partial_t^{(k)}\mathbf{Q}(x_d, 0)]\frac{\tau^k}{k!}. \tag{65}$$

The functions $\mathbf{G}^{(k)}$ in (7) are now functions of space derivatives of the reconstruction polynomial $\mathbf{P}_i(x)$ and thus

$$\mathbf{Q}_i(x_d,\tau) = \mathbf{P}_i(x_d) + \sum_{k=1}^{K}[\mathbf{G}^{(k)}(\mathbf{P}_i^{(0)}(x_d),\mathbf{P}_i^{(1)}(x_d),\ldots,\mathbf{P}_i^{(k)}(x_d))]\frac{\tau^k}{k!}. \tag{66}$$

With this information available the space-time integral average can be computed to any desired order of accuracy.

4.2. Analogy with second-order schemes

The second order version of the ADER schemes reported in [40] is analogous to the GRP scheme of Ben-Artzi and Falcovitz [1]. In fact the scheme of [40] is a modification of the GRP scheme, whereby the computation of the time derivative in the power series expansion (to second order) for the solution of the DRP is reduced to computing the solution of a linearized Riemann problem for spatial gradients. The higher order ADER schemes are a straight generalization of this modified GRP scheme. As seen in previous sections, the numerical flux is computed at the solution of the Derivative Riemann Problem at the interface, which is found as a power series expansion right at the interface $x = 0$, as a function of time.

Similarly, the method of Harten et al. [17] in its second-order mode (for the homogeneous case) may be seen as a way of interpreting the second order MUSCL-Hancock scheme [48], the numerical flux of which is

$$\mathbf{F}_{i+\frac{1}{2}}^{MH} = \mathbf{F}_{i+\frac{1}{2}}^{MH}(\widetilde{\mathbf{Q}}_i^R,\widetilde{\mathbf{Q}}_{i+1}^L) = \mathbf{F}(\widetilde{\mathbf{Q}}_{i+\frac{1}{2}}(0)), \tag{67}$$

where $\widetilde{\mathbf{Q}}_{i+\frac{1}{2}}(x/t)$ is the similarity solution of the classical Riemann problem

$$\left.\begin{array}{ll} \text{PDEs:} & \partial_t\mathbf{Q} + \partial_x\mathbf{F}(\mathbf{Q}) = \mathbf{0}, \quad x\in(-\infty,\infty), \quad t>0, \\ \text{IC:} & \mathbf{Q}(x,0) = \begin{cases} \widetilde{\mathbf{Q}}_i^R & \text{if } x<0, \\ \widetilde{\mathbf{Q}}_{i+1}^L & \text{if } x>0, \end{cases} \end{array}\right\} \tag{68}$$

with

$$\left.\begin{array}{l} \widetilde{\mathbf{Q}}_i^R = \mathbf{Q}_i^R - \frac{1}{2}\frac{\Delta t}{\Delta x}[\mathbf{F}(\mathbf{Q}_i^R) - \mathbf{F}(\mathbf{Q}_i^L)], \\ \widetilde{\mathbf{Q}}_{i+1}^L = \mathbf{Q}_{i+1}^L - \frac{1}{2}\frac{\Delta t}{\Delta x}[\mathbf{F}(\mathbf{Q}_{i+1}^R) - \mathbf{F}(\mathbf{Q}_{i+1}^L)], \end{array}\right\} \tag{69}$$

and

$$\mathbf{Q}_i^R = \mathbf{Q}_i^n + \frac{1}{2}\Delta x\boldsymbol{\Delta}_i, \quad \mathbf{Q}_{i+1}^L = \mathbf{Q}_{i+1}^n - \frac{1}{2}\Delta x\boldsymbol{\Delta}_{i+1}. \tag{70}$$

Here $\boldsymbol{\Delta}_i$ and $\boldsymbol{\Delta}_{i+1}$ are the slopes in the MUSCL reconstruction in cells i and $i+1$ respectively. Note the relations

$$\boldsymbol{\Delta}_i = \frac{\mathbf{Q}_i^R - \mathbf{Q}_i^L}{\Delta x} = \mathbf{P}_i', \quad \boldsymbol{\Delta}_{i+1} = \frac{\mathbf{Q}_{i+1}^R - \mathbf{Q}_{i+1}^L}{\Delta x} = \mathbf{P}_{i+1}'. \tag{71}$$

On the other hand, a second-order method with the HEOC solver, see (18), (19), has flux

$$\mathbf{F}_{i+\frac{1}{2}} = \mathbf{F}_{i+\frac{1}{2}}\left(\widetilde{\mathbf{Q}}_L\left(\frac{1}{2}\Delta t\right),\widetilde{\mathbf{Q}}_R\left(\frac{1}{2}\Delta t\right)\right) = \mathbf{F}\left(\mathbf{D}\left(\frac{1}{2}\Delta t,0\right)\right). \tag{72}$$

See (27). From (18) and (19) we have

$$\left.\begin{array}{l} \widetilde{\mathbf{Q}}_L(\frac{1}{2}\Delta t) = \mathbf{P}_i(0_-) - \frac{1}{2}\Delta t\mathbf{A}_L\ \mathbf{P}_i'(0_-), \\ \widetilde{\mathbf{Q}}_R(\frac{1}{2}\Delta t) = \mathbf{P}_{i+1}(0_+) - \frac{1}{2}\Delta t\mathbf{A}_R\ \mathbf{P}_{i+1}'(0_+), \end{array}\right\} \tag{73}$$

with

$$\mathbf{A}_L = \mathbf{A}(\mathbf{Q}_L(0_-)), \quad \mathbf{A}_R = \mathbf{A}(\mathbf{Q}_R(0_+)). \tag{74}$$

For a linear system with constant coefficient matrix $\widehat{\mathbf{A}}$ we have $\mathbf{F}(\mathbf{Q}) = \widehat{\mathbf{A}}\mathbf{Q}$ and one sees that the left and right states in (68) are identical to those in (73) and thus the second order ADER scheme based on the HEOC solver is identical to the MUSCL-Hancock scheme.

The schemes are not identical for non-linear systems but the analogy just discussed provides an interpretation to the rather *enigmatic* evolution step (69) of the boundary extrapolated values by half a time step, in the MUSCL-Hancock method [48].

Thus, from the numerical point of view, we can interpret the numerical method of Harten et al. [17] as being a high-order generalization of the MUSCL-Hancock second order method. Similarly, the ADER method, with any of the DRP solvers studied here, may be interpreted as a high-order generalization of the second order method of Ben-Artzi and Falcovitz [1], following its modification reported in [40].

Corresponding finite volume schemes in two space dimensions using unstructured meshes are described in Section 6.

5. Tests for the derivative Riemann problem solvers

In this section we assess the performance of the Derivative Riemann Problem solvers studied in the paper via a series of test problems for the Euler equations of gas dynamics and for the shallow water equations with source terms. As no exact solutions are known for the class of test problems of interest here, we obtain reference solutions by computing solutions numerically. To this end we use three numerical methods, the first-order Godunov method, the second-order MUSCL-Hancock method and the Random Choice Method (RCM) [13], all of them applied on a very fine mesh.

We note that RCM has the unique property of being able to resolve the very-early time evolution of the solution in a way that no other method known to us can do. This is important, as the proposed DRP solvers are assessed in their domain of validity, namely for short times. For test problems involving an initial discontinuity, most methods will require a fairly large number of time steps to gradually begin to establish the structure of the true solution. Moreover, the early-time numerical results may exhibit large unphysical oscillations, even when monotone (for the scalar case) schemes are used. To illustrate this point we solve a simple shock-tube problem for the Euler equations in the domain $[-1, 1]$, with initial data $\rho_L = 1, u_L = 3/4, p_L = 1$ for $x < 0$ and $\rho_R = 1/8, u_R = 0, p_R = 1/10$ for $x > 0$.

Fig. 4 shows the exact (full line) and numerical solutions (symbols) at time $t = 0.015$ using the Godunov first-order method (circles), the MUSCL-Hancock method (squares) and the RCM method (triangles). For all three numerical methods we use the exact Riemann solver. For the first two methods we use $C_{cfl} = 0.9$ and for RCM we use $C_{cfl} = 0.45$. Fig. 4 shows only the region close to the position of the discontinuities at time $t = 0$. For the output time considered the Godunov and MUSCL-Hancock methods do only four time steps and RCM nine time steps. The first two methods are unable to resolve the wave structure correctly. RCM finds all intermediate states correctly. This property of RCM is useful to our purpose.

Recall that the DRP solution is valid precisely at the interface $x = 0$, as a function of time. The numerical methods give the approximate solution in every cell of the mesh that discretizes the domain $[-1, 1]$. For any mesh used one always has, at any time, one value (vector) immediately to the left of $x = 0$ and one immediately to the right of $x = 0$. To extract the sought reference solution at a given time we solve the classical Riemann problem for these two neighbouring states and pick up the solution right at the interface $x = 0$. This is the *reference numerical* solution that we compare with the DRP solutions.

The series of test problems includes a simple test (Test 1) with smooth initial condition throughout, no discontinuities in the data are present. A second test (Test 2) has no jump discontinuities in the state variables but admits discontinuities in derivatives at the interface. Other more demanding test problems are constructed from Test 2, by adding a discontinuity in pressure. Four new cases are thus generated by varying the strength of the initial pressure jump $\Delta p = (p_L - p_R)/p_R$ at the interface, namely $\Delta p = 0.01$, $\Delta p = 0.1, \Delta p = 1.0$ and $\Delta p = 10.0$. For these four cases with an initial jump discontinuity the reference numerical solution used is that obtained by the Random Choice Method, on a very fine mesh. Finally

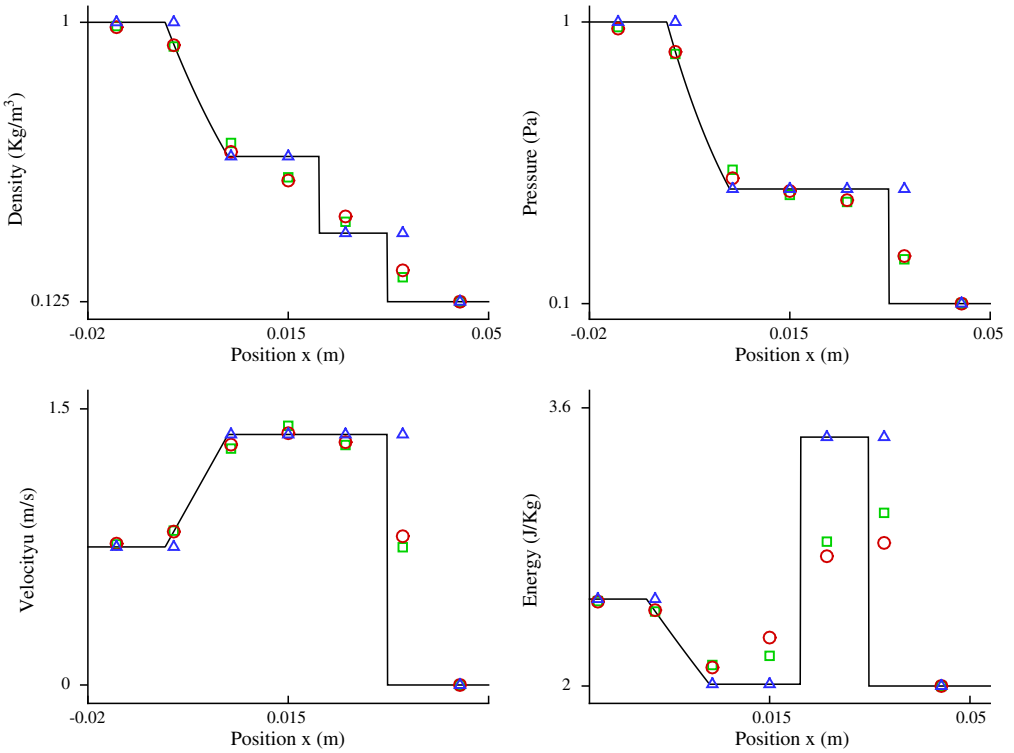

Fig. 4. Shock-tube test problem. Exact (full line) and numerical solutions (symbols) at time $t = 0.015$ using the Godunov first-order method (circles), the MUSCL-Hancock method (squares) and the random choice method (triangles).

a third test (Test 3) is constructed for the shallow water equations with source terms. This test shows the DRP solution for a system of non-linear balance laws.

5.1. Test 1: smooth initial conditions

The initial conditions

$$\left.\begin{aligned} \rho(x,0) &= 1 + \tfrac{4}{5}\sin\left(\tfrac{\pi x}{2}\right) + \tfrac{1}{10}\sin\left(\tfrac{5\pi x}{2}\right), \\ u(x,0) &= \tfrac{1}{2}\left(x - \tfrac{1}{2}\right)^4, \\ p(x,0) &= 10 + 2x^4. \end{aligned}\right\} \tag{75}$$

are smooth throughout; there are no jumps in state or derivatives at $x = 0$. In this particular case all three DRP solvers give, algebraically, the same solution.

In Fig. 5 we present the solution of the DRP problem up to fifth order (DRP_4) for all three components of the vector $\mathbf{Q} = [\rho, \rho u, E] \equiv [q_1, q_2, q_3]$, where ρ is density, u is particle velocity and E is total energy. As expected, by increasing the order, the DRP solution approximates the reference solution very well. The DRP_0 solution is constant in time and the DRP_1 solution is linear in time. We note that the approximation improves with the order, which is verified for all three components q_1, q_2 and q_3. For q_2 the DRP_1 solution is practically identical to the DRP_0 solution. This is correct in the sense that at the time $\tau = 0_+$ the slope of the reference solution is close to zero and the linear characteristic of the DRP_1 solution will not modify this slope. Table 1 shows the error in the L_2 norm at different times. The main feature of these errors is that as time decreases the error decreases and as the order of accuracy increases the error decreases, as expected.

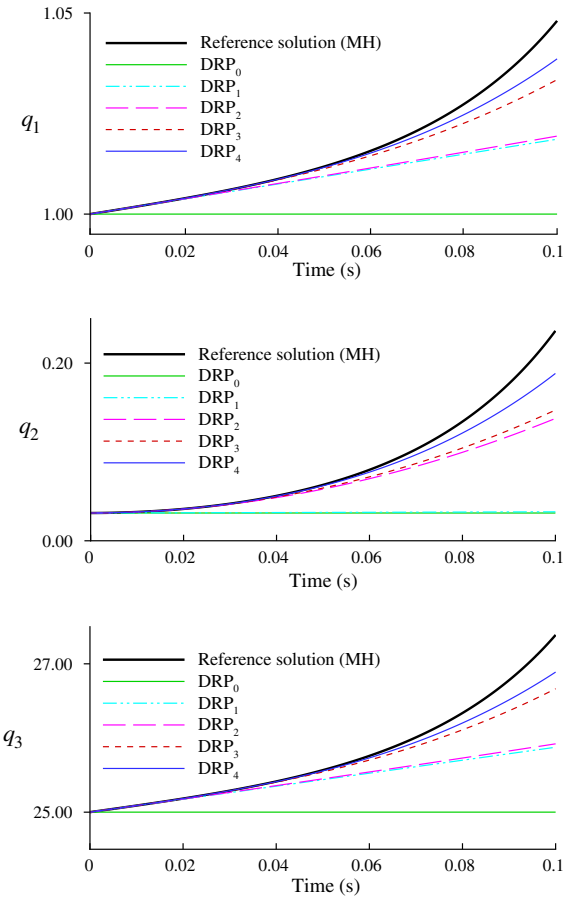

Fig. 5. Test 1: DRP solution for $q_1 = \rho, q_2 = \rho u$ and $q_3 = E$. Thick line is the reference solution.

Table 1
Test 1: Errors in the L_2-norm for the vector $\mathbf{Q}$

Order	$t = 0.0125$	$t = 0.0250$	$t = 0.0500$	$t = 0.1000$
DRP_0	1.1165×10^{-1}	2.3454×10^{-1}	5.6704×10^{-1}	2.3979×10
DRP_1	2.7922×10^{-3}	1.7078×10^{-2}	1.3222×10^{-1}	1.5275×10
DRP_2	1.5193×10^{-3}	1.2754×10^{-2}	1.1715×10^{-1}	1.4712×10
DRP_3	6.8953×10^{-5}	1.1577×10^{-3}	2.4454×10^{-2}	7.3055×10^{-1}
DRP_4	1.3276×10^{-5}	2.6653×10^{-4}	1.0205×10^{-2}	5.0280×10^{-1}

5.2. Test 2: initial data with discontinuous derivatives

Test 2 has piece-wise smooth initial conditions that are continuous at $x = 0$ but with discontinuous derivatives at $x = 0$, see (76). For this test problem all three DRP solvers (TT, CT and HEOC) agree quite well for the very early times but differ quite visibly for larger times. Fig. 6 shows the fifth-order (DRP_4) solution for the three solvers, for each component of the vector $\mathbf{Q}$. For the first and third components the solver CT is the most accurate, followed by HEOC. For the second component of $\mathbf{Q}$, the TT solver gives better results. More comprehensive information about the relative merits of the three solvers is given in Tables 2–4, where errors measured in the L_2-norm are displayed. For time $t = 0.0250$, the error of the DRP_4 solution for the TT solver is 1.3295584×10^{-2}, for the HEOC solver is 7.3686016×10^{-3} and

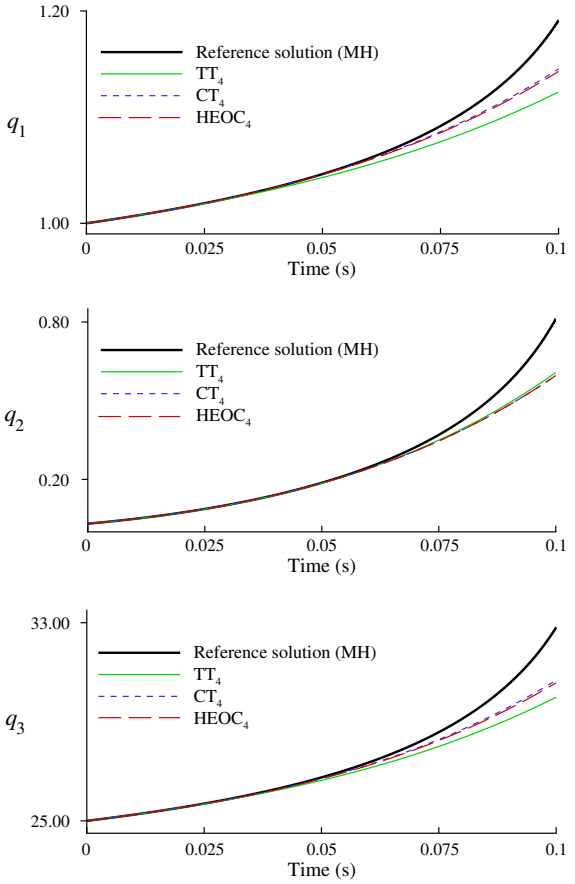

Fig. 6. Fifth order DRP solutions for Test 2, using TT, CT and HEOC for the three components of **Q**.

for the CT solver is 5.1386851×10^{-3}. A general conclusion is that for all three solvers the error diminishes as the order increases, while the solution is more accurate for small times, and for which they all tend to agree.

$$\left.\begin{aligned}
\rho_L(x,0) &= 1.433903078 + \tfrac{4}{5}\sin\left(\tfrac{\pi(x-0.3)}{2}\right) + \tfrac{1}{10}\sin\left(\tfrac{5\pi(x-0.3)}{2}\right)\\
u_L(x,0) &= \tfrac{1}{2}\left(x-\tfrac{4}{5}\right)^4 - 0.17355\\
p_L(x,0) &= 9.9838 + 2(x-0.3)^4\\
\rho_R(x,0) &= 1 + \tfrac{4}{5}\sin\left(\tfrac{\pi x}{2}\right) + \tfrac{1}{10}\sin\left(\tfrac{5\pi x}{2}\right)\\
u_R(x,0) &= \tfrac{1}{2}\left(x-\tfrac{1}{2}\right)^4\\
p_R(x,0) &= 10 + 2x^4
\end{aligned}\right\} \tag{76}$$

Table 2
Test 2: Errors in the L_2-norm for the vector **Q** for the Toro–Titarev solver

Order	$t = 0.0125$	$t = 0.0250$	$t = 0.0500$	$t = 0.1000$
DRP_0	3.1847×10^{-1}	6.9922×10^{-1}	1.7616×10	7.8567×10
DRP_1	2.4316×10^{-2}	1.1101×10^{-1}	5.8542×10^{-1}	5.5045×10
DRP_2	3.5714×10^{-3}	2.8047×10^{-2}	2.5371×10^{-1}	4.1782×10
DRP_3	1.9815×10^{-3}	1.5386×10^{-2}	1.5270×10^{-1}	3.3683×10
DRP_4	1.8509×10^{-3}	1.3295×10^{-2}	1.1931×10^{-1}	2.8327×10

Table 3
Test 2: Errors in the L_2-norm for the vector $\mathbf{Q}$ for the HEOC solver

Order	$t = 0.0125$	$t = 0.0250$	$t = 0.0500$	$t = 0.1000$
DRP_0	3.1847×10^{-1}	6.9922×10^{-1}	1.7616×10	7.8567×10
DRP_1	2.4686×10^{-2}	1.1249×10^{-1}	5.9124×10^{-1}	5.5272×10
DRP_2	4.7040×10^{-3}	3.2947×10^{-2}	2.7609×10^{-1}	4.2905×10
DRP_3	1.7812×10^{-3}	9.5614×10^{-3}	8.9178×10^{-2}	2.7972×10
DRP_4	1.6440×10^{-3}	7.3686×10^{-3}	5.4229×10^{-2}	2.2544×10

Table 4
Test 2: Errors in the L_2-norm for the vector $\mathbf{Q}$ for the Castro–Toro solver

Order	$t = 0.0125$	$t = 0.0250$	$t = 0.0500$	$t = 0.1000$
DRP_0	3.1847×10^{-1}	6.9922×10^{-1}	1.7616×10	7.8567×10
DRP_1	2.4316×10^{-2}	1.1101×10^{-1}	5.8542×10^{-1}	5.5045×10
DRP_2	4.2460×10^{-3}	3.0772×10^{-2}	2.6462×10^{-1}	4.2213×10
DRP_3	1.3222×10^{-3}	7.3435×10^{-3}	7.7090×10^{-2}	2.7221×10
DRP_4	1.1853×10^{-3}	5.1386×10^{-3}	4.1429×10^{-2}	2.1497×10

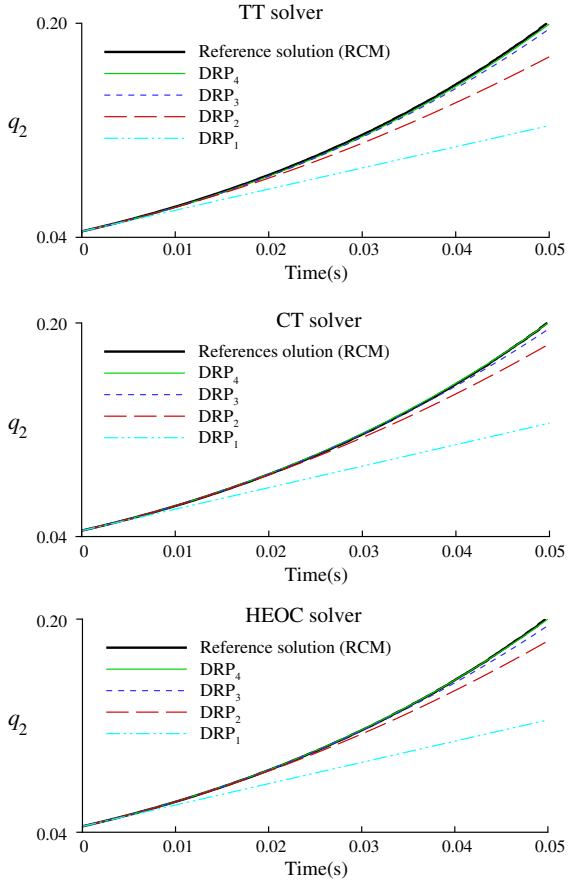

Fig. 7. DRP solution for TT, CT and HEOC solvers for $\Delta p = 0.01$. Thick full line is the reference solution obtained with the RCM method.

5.3. Tests with discontinuous initial conditions

The tests of this section are generated from the initial conditions of Test 2 by adding a term in $p_L(x,0)$ and thus generating a jump $\Delta p = (p_L(0,0) - p_R(0,0))/p_R(0,0)$ in pressure at $x = 0$. We consider four cases by taking Δp with values $0.01, 0.1, 1.0, 10.0$.

Results are shown in Figs. 7–10. Fig. 7 displays results for $\Delta p = 0.01$, with a small pressure jump; the DRP solution improves as the order increases, for all three solvers. In Fig. 8, for $\Delta p = 0.10$, the solution from the TT solver improves as the order increases. The situation is different for the CT and HEOC solvers, whose solutions cross the reference solution.

Results for $\Delta p = 1.00$ are shown in Fig. 9. Here the Toro–Titarev solver seems to perform better but note that when the order increases to DRP_4, it misrepresents the curvature and thus crosses the reference solution. The solutions of the present solvers CT and HEOC show wrong initial slopes. As the order increases the curvature seems to approximate the curvature of the reference solution better, with the HEOC solution being closer to the reference solution than that of CT. For both the CT and HEOC solvers the second order solution crosses the reference solution.

Fig. 10 shows the DRP solutions for $\Delta p = 10.0$. All three solvers give the wrong initial slope. Their failure to agree with the reference solution increases dramatically as the initial pressure jump becomes larger. Moreover, they fail to capture the initial slope and the behaviour of the reference solution.

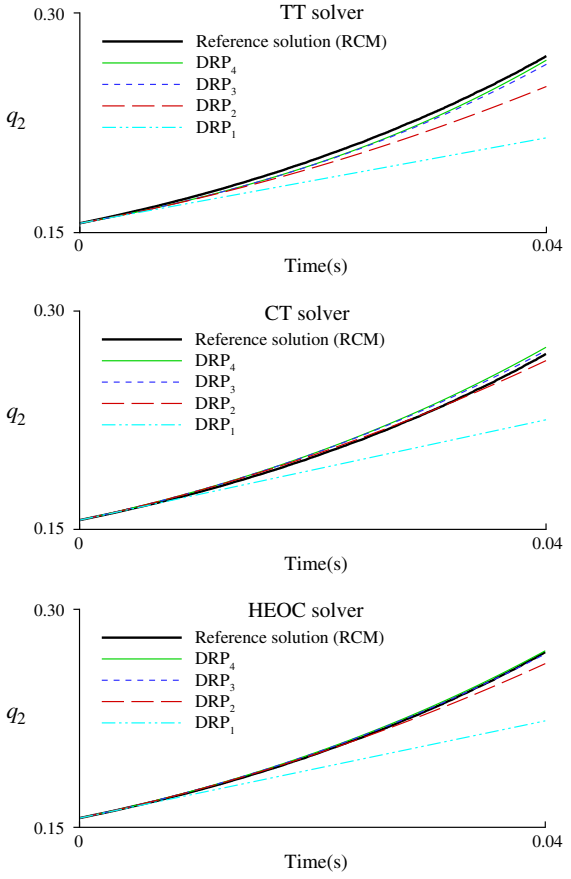

Fig. 8. DRP solution for TT, CT and HEOC solvers for $\Delta p = 0.10$. Thick full line is the reference solution obtained with the RCM method.

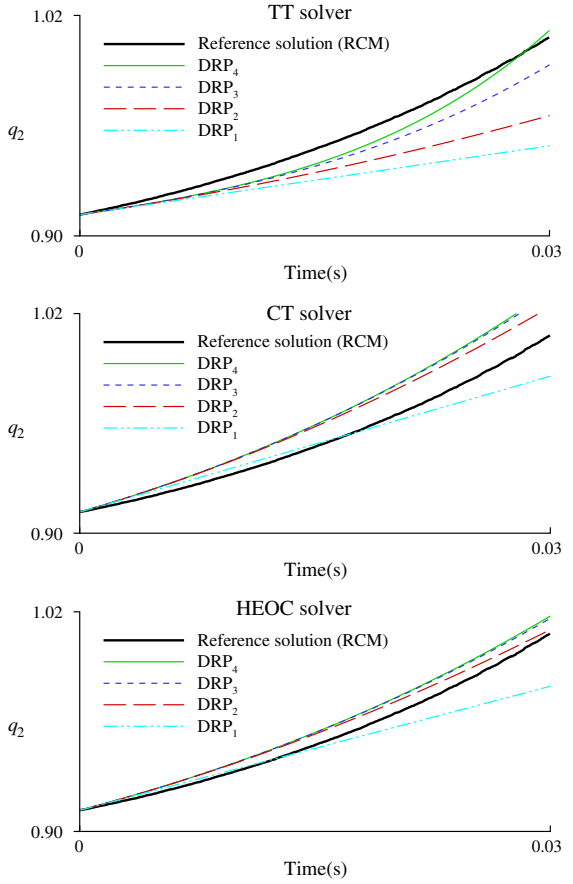

Fig. 9. DRP solution for TT, CT and HEOC solvers for $\Delta p = 1.00$. Thick full line is the reference solution obtained with the RCM method.

5.4. Test 3: shallow water equations with source terms

For this test problem we utilize the shallow water equations with a source term

$$\partial_t \mathbf{Q} + \partial_x \mathbf{F}(\mathbf{Q}) = \mathbf{S}(\mathbf{Q}), \tag{77}$$

with

$$\mathbf{Q} = \begin{pmatrix} h \\ hu \end{pmatrix}, \quad \mathbf{F}(\mathbf{Q}) = \begin{pmatrix} hu \\ hu^2 + \frac{1}{2}gh^2 \end{pmatrix}, \quad \mathbf{S}(\mathbf{Q}) = \begin{pmatrix} 0 \\ -ghb_x \end{pmatrix}. \tag{78}$$

Here $h(x,t)$ is water depth, $u(x,t)$ is particle velocity, $h(x)$ is (prescribed) bottom elevation above a horizontal datum and g is acceleration due to gravity. The total free surface elevation is $H(x,t) = h(x,t) + b(x)$. The source term accounts for the variation of the bed elevation. See Fig. 11. For background on the shallow water equations see for example [43].

The initial conditions for h and u and the prescribed bed profile for the test are

$$\left.\begin{aligned} h(x,0) &= 1.5 + 0.5x + x^2 \\ u(x,0) &= 1.0 + x \\ b(x) &= 0.5 - 0.3x^3 \end{aligned}\right\} \tag{79}$$

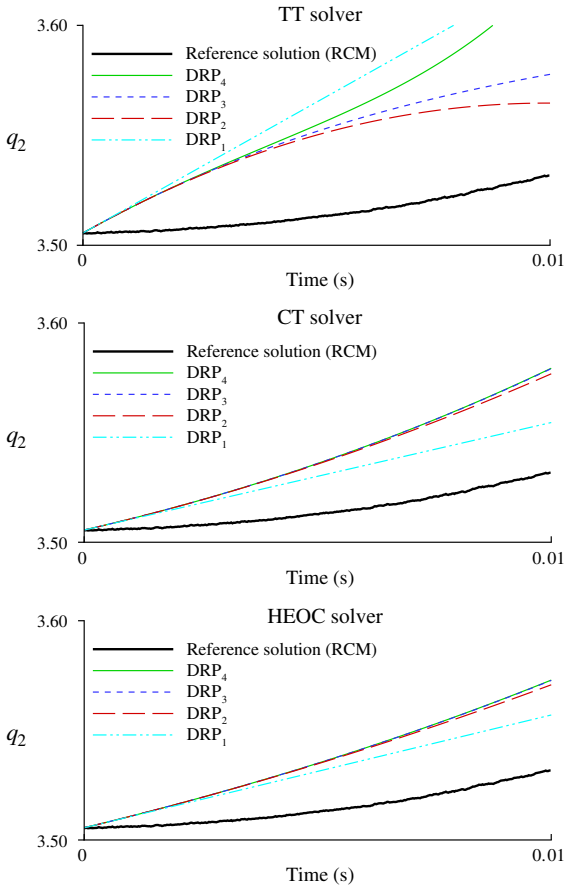

Fig. 10. DRP solution for TT, CT and HEOC solvers for $\Delta p = 10.0$. Thick full line is the reference solution obtained with the RCM method.

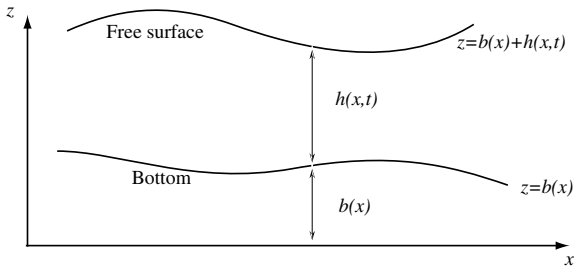

Fig. 11. Reference coordinate system for bed $b(x)$ and free surface elevation $H(x,t) = b(x) + h(x,t)$.

In Fig. 12 we present solutions of the DRP upto fifth order (DRP_4) for both components of the unknown vector $\mathbf{Q} = [h, hu] \equiv [q_1, q_2]$. As expected, by increasing the order, the DRP solution approximates the reference solution very accurately.

5.5. Discussion of results

Recall that the main purpose of solving the Derivative Riemann Problem (DRP) is to provide a time-dependent solution at each cell interface, from which a corresponding numerical flux can be found and used in the

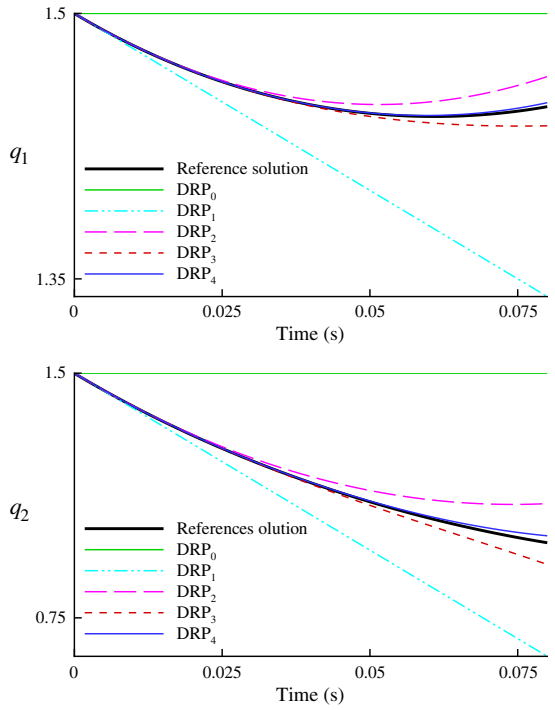

Fig. 12. Test 3: Shallow water equations with source terms. DRP solution for $q_1 = h$ and $q_2 = hu$. Thick line is the reference solution.

context of finite volume methods or discontinuous Galerkin finite element methods. However, before considering numerical methods we focus the discussion on the solution of the particular Cauchy problem, the DRP. There are a number of aspects of the solution procedure of the DRP that warrant a detailed discussion.

One issue concerns the time evolution of the initial data, as done in the HEOC solver, and of the solution, as done in the TT and CT solvers. We have observed that even when the initial condition consists of physically admissible data, it is possible that the time evolution yields unphysical values, such as negative densities. This appears to be more crucial for the HEOC solver, because it could happen that, at a given time, the time evolved data contains unphysical values, which then the appropriate (classical) Riemann solver rejects, leading to a failure of the scheme. The TT and CT solvers appear to be less sensitive to this problem. These two solvers evolved in time the sought solution right at the interface. The corresponding time-dependent solution may still include unphysical values. However, since these are then only used in the numerical integration to obtain the flux it is possible that the scheme may continue to function.

Stationary discontinuities in the solution of the DRP represent another situation where differences between the various solvers exist. The TT and CT solvers expand the solution at the interface starting from a leading term computed a time $t = 0_+$ that dominates the evolution. In the presence of a stationary discontinuity at $t = 0_+$ there are two possible choices for the leading term. For the first-order mode of the methods, it does not matter which of the two states is taken, as these satisfy the Rankine–Hugoniot conditions and therefore the respective fluxes are identical. For the higher-order version of the methods the situation is not clear. There will be two different time expansions, depending on which side is taken as the leading term. This non-uniqueness remains so even if the discontinuity moves for times $t > 0$. We have performed some numerical tests on the effect of choosing from the two available expansions. There is an observable numerical difference but, at least for the tests performed, it is very small and as time evolves it virtually vanishes. Still, this is an aspect of the TT and CT methods that would benefit from further investigations. On the other hand, the HEOC method is less sensitive to this problem. In particular, if the discontinuity positioned at the origin, at the early times, then moves as time increases. The HEOC has the mechanism to capture this behaviour.

In general, boundary conditions are a challenging problem in the context of high-order numerical methods. For example, for reflecting boundary conditions we *solve* an inverse Riemann problem, in the sense that we

need to identify appropriate initial conditions such that the Riemann problem solution at the boundary reproduces what is physically sought, for example, zero velocity. To this purpose the HEOC solver appears more attractive than the TT and CT solvers, as it is very simple to create, at each time, in the time evolution process, the appropriate data states to match the desired condition.

Some comments regarding computational cost are in order. The HEOC solver needs a *robust* Riemann solver for each *time-integration point* τ, within the time step $0 \leqslant \tau \leqslant \Delta t$. This can be time-consuming, as a robust Riemann solver will in general be a non-linear Riemann solver. In addition, the HEOC solver requires the development of two series expansions, one on each side of the interface. The TT solver, on the other hand, requires a single expansion right at the interface. Moreover, in the TT and CT solvers, one uses a non-linear Riemann solver only once, in order to compute the leading term reliably.

A rather surprising observation resulting from the present work is that, from the evidence available, all three DRP solvers are unable to resolve correctly the DRP problem for the case of *non-linear systems with large jumps*. This is different from the case of linear systems with constant coefficients, for which all three methods have been proved to be exact if the polynomial data are of finite degree. The situation is also different from the scalar non-linear inhomogeneous case; in [46] it is (empirically) shown that the Toro–Titarev solver gives the correct solution for initial jumps of any size. However, from the results of the present work, this property does not seem to carry to non-linear systems.

On the other hand, the available experience, see for example [38,11], shows that the high-order ADER schemes for non-linear systems based on the solution of the Derivative Riemann Problem are indeed capable of reproducing the theoretically expected orders of accuracy. Obviously, the corresponding convergence rate tests are performed for smooth solutions. However, even for smooth solutions the local reconstruction procedure will necessarily produce jumps at the interfaces. Obviously these jumps are small in this case and are possibly within the range for which the existing DRP solvers yield the correct approximation.

6. ADER methods in one and two space dimensions

The purpose of this section is to briefly outline the construction of ADER high-order finite volume methods in one and two space dimensions, using the solution of the DRP, and to illustrate the performance of such numerical schemes.

First we solve the Euler equations of gas dynamics in two space dimensions using unstructured meshes and study two problems. The first one is used to perform a convergence rates study and to show that the theoretically expected high order of accuracy is actually verified in practice, at least for the chosen test problem. The second test is used to illustrate the fact that the proposed schemes can be used to solve realistic problems involving shock waves in complicated, non-cartesian geometries.

Then we solve the shallow water equations in one space dimension with a source term due to bottom elevation. The purpose here is to address the issue of *balance* between flux and source terms near the steady state in the context of ADER schemes. Through an example we show that the ADER schemes may be termed asymptotically well-balanced; we also show through an example that the expected convergence rates are verified for balance laws.

6.1. Euler equations and finite volume schemes on triangular meshes

We solve the two-dimensional compressible Euler equations

$$\frac{\partial}{\partial t}\mathbf{Q} + \frac{\partial}{\partial x}\mathbf{F}(\mathbf{Q}) + \frac{\partial}{\partial y}\mathbf{G}(\mathbf{Q}) = \mathbf{0}, \tag{80}$$

with

$$\mathbf{Q} = \begin{pmatrix} \rho \\ \rho u \\ \rho v \\ E \end{pmatrix}, \quad \mathbf{F}(\mathbf{Q}) = \begin{pmatrix} \rho u \\ \rho u^2 + p \\ \rho uv \\ u(E+p) \end{pmatrix}, \quad \mathbf{G}(\mathbf{Q}) = \begin{pmatrix} \rho v \\ \rho uv \\ \rho v^2 + p \\ v(E+p) \end{pmatrix} \tag{81}$$

and the polytropic equation of state, with the specific internal energy given as $e(\rho,p)=\frac{p}{\rho(\gamma-1)}$. Here ρ is density, u,v are x and y components of velocity, p is pressure and E is the total energy, defined as $E=\rho(\frac{1}{2}(u^2+v^2)+e(\rho,p))$. For the calculations of this paper we take $\gamma=1.4$, as for air.

The schemes are constructed by considering a control volume T_m in a two-dimensional domain, where T_m is an element of a conformal triangulation of the full spatial domain Ω. Writing equations (80) in divergence form

$$\mathbf{Q}_t+\nabla\mathbf{H}(\mathbf{Q})=\mathbf{0},\quad \mathbf{H}(\mathbf{Q})=[\mathbf{F}(\mathbf{Q}),\mathbf{G}(\mathbf{Q})]^{\mathrm{T}} \tag{82}$$

and integrating over the triangle T_m in space and time we obtain

$$\mathbf{Q}_m^{n+1}=\mathbf{Q}_m^n-\frac{\Delta t}{|T_m|}\sum_{j=1}^{3}\mathbf{H}_{m,j}^n. \tag{83}$$

Here $\mathbf{H}_{m,j}^n$ is the numerical flux across the edge j of the triangle T_m, $|T_m|$ is the area of triangle T_m and $\mathbf{Q}_m^n$ is the cell average

$$\mathbf{Q}_m^n=\frac{1}{|T_m|}\int_{T_m}\mathbf{Q}(\mathbf{x},t^n)\mathrm{d}\mathbf{x}. \tag{84}$$

Once the numerical flux across the edges of the triangle are defined we obtain an explicit one-step numerical method. The numerical flux $\mathbf{H}_{m,j}^n$ for edge j is obtained by integrating along the edge $\partial T_{m,j}$ in the time interval $[t^n,t^{n+1}]$,

$$\mathbf{H}_{m,j}^n=\frac{1}{\Delta t}\int_{t^n}^{t^{n+1}}\int_{\partial T_{m,j}}\mathbf{F}(\mathbf{Q}(\mathbf{x},\tau))\cdot\mathbf{n}\mathrm{d}\mathbf{x}\,\mathrm{d}\tau, \tag{85}$$

which is approximated as

$$\mathbf{H}_{m,j}^n=\sum_{k=1}^{N^t}\omega_k^t|\partial T_{m,j}|\sum_{h=1}^{N^x}\omega_h^x\mathbf{F}(\mathbf{Q}(\boldsymbol{x}_h,t_k))\cdot\mathbf{n}. \tag{86}$$

The integral (85) is calculated by a Gaussian quadrature of the desired order defining the quadrature points $\boldsymbol{x}_h$ and t_k and the weights ω_h^x and ω_k^t, with $\boldsymbol{x}_h\in\partial T_{m,j}$ and $t_k\in[t^n,t^{n+1}]$. At each spatial integration point $\boldsymbol{x}_h$ we set locally a Derivative Riemann Problem (1) to obtain the vector $\mathbf{Q}(\boldsymbol{x}_h,t_k)=\mathbf{Q}_{LR}(t_k)$ as in (3), see Fig. 13. $\mathbf{Q}_{LR}(\tau)$ can be obtained by using any of the three DRP solvers studied in this paper. Recall that the basic information available in finite volume schemes is a set of cell averages and therefore in order to produce a high-order representation of the data in each cell we need to perform a reconstruction procedure to obtain the data for (1). Here we apply the reconstruction procedure reported in [8], which extends the ideas of the ENO/WENO techniques [20] combined with the sectorial stencil of [23] and the use of orthogonal basis functions from the discontinuous Galerkin methodology. See also [11].

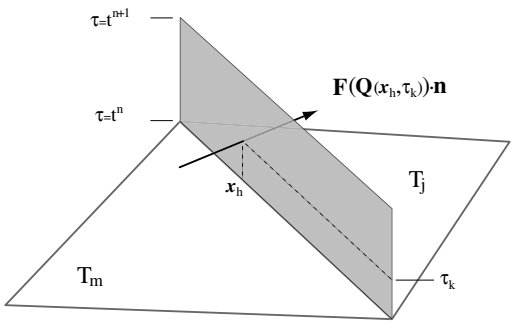

Fig. 13. Numerical flux computed at the Gaussian point $\boldsymbol{x}=\boldsymbol{x}_h$ and $t=t_k$.

6.1.1. Convergence rate studies

For the purpose of studying the convergence rates of the schemes we adopt the test problem proposed in [19], which consists of a convected isentropic vortex computed in a square domain, with periodic boundary conditions. The initial condition consists of a mean constant flow modified by an isentropic perturbation. The initial mean flow is given by $\rho = 1, p = 1$ and $(u, v) = (1, 1)$ and the perturbation is given by

$$\left.\begin{aligned} \delta u &= -\tfrac{\epsilon}{2\pi} e^{\frac{1}{2}(1-r^2)} y, \\ \delta v &= \tfrac{\epsilon}{2\pi} e^{\frac{1}{2}(1-r^2)} x, \\ \delta \rho &= (1+\delta T)^{\frac{1}{\gamma-1}} - 1, \\ \delta p &= (1+\delta T)^{\frac{\gamma}{\gamma-1}} - 1, \\ \delta T &= -\tfrac{(\gamma-1)\epsilon^2}{8\gamma\pi^2} e^{1-r^2}, \end{aligned}\right\} \tag{87}$$

where $r^2 = x^2 + y^2, \epsilon = 5$ (the vortex strength). The computational domain is $[-5, 5] \times [-5, 5]$ discretized by an unstructured mesh of triangles.

Tables 5–8 give errors and convergence rates for the finite volume ADER schemes using the CT (present) derivative Riemann problem solver. Schemes up to fifth order of accuracy are considered, on four levels of

Table 5
Convergence rates test: second order method

Mesh	L_1 error	O_1	L_2 error	O_2	L_∞ error	O_∞
224	2.47×10		5.67×10^{-1}		4.43×10^{-1}	
898	1.42×10	0.85	3.42×10^{-1}	0.78	2.82×10^{-1}	0.69
3618	3.43×10^{-1}	2.03	8.19×10^{-2}	2.04	8.71×10^{-2}	1.67
14402	5.84×10^{-2}	2.56	1.37×10^{-2}	2.58	1.51×10^{-2}	2.53
57694	7.65×10^{-3}	2.99	1.37×10^{-3}	3.11	4.22×10^{-3}	1.88

Table 6
Convergence rates test: third order method

Mesh	L_1 error	O_1	L_2 error	O_2	L_∞ error	O_∞
224	2.29×10		5.23×10^{-1}		4.11×10^{-1}	
898	7.35×10^{-1}	1.75	1.65×10^{-1}	1.77	1.30×10^{-1}	1.77
3618	1.02×10^{-1}	2.82	2.49×10^{-2}	2.70	1.94×10^{-2}	2.71
14402	1.60×10^{-2}	2.67	4.03×10^{-3}	2.63	2.84×10^{-3}	2.78
57694	2.06×10^{-3}	3.02	5.21×10^{-4}	3.01	3.64×10^{-4}	3.03

Table 7
Convergence rates test: fourth order method

Mesh	L_1 error	O_1	L_2 error	O_2	L_∞ error	O_∞
224	2.14×10		4.87×10^{-1}		3.88×10^{-1}	
898	3.76×10^{-1}	2.68	6.23×10^{-2}	3.17	5.03×10^{-2}	3.14
3618	1.67×10^{-2}	4.43	3.50×10^{-3}	4.10	3.87×10^{-3}	3.65
14402	1.12×10^{-3}	3.91	2.25×10^{-4}	3.97	2.48×10^{-4}	3.97
57694	6.84×10^{-5}	4.12	1.37×10^{-5}	4.12	1.61×10^{-5}	4.03

Table 8
Convergence rates test: fifth order method

Mesh	L_1 error	O_1	L_2 error	O_2	L_∞ error	O_∞
224	1.95×10		4.60×10^{-1}		3.71×10^{-1}	
898	3.86×10^{-1}	2.49	7.19×10^{-2}	2.85	6.99×10^{-2}	2.57
3618	2.90×10^{-2}	3.69	7.23×10^{-3}	3.27	8.40×10^{-3}	3.02
14402	1.31×10^{-3}	4.48	3.44×10^{-4}	4.40	2.12×10^{-4}	5.32
57694	1.48×10^{-5}	6.60	3.85×10^{-6}	6.62	2.54×10^{-6}	6.52

mesh refinement. Errors are measured in three norms L_1, L_2, L_∞ and the corresponding empirical orders of accuracy are O_1, O_2 and O_∞. The expected orders of accuracy are reached in all cases.

6.1.2. Shock wave reflection problem

The purpose of this test is simply to illustrate the potential of the methods presented to solve realistic problems to high accuracy on complicated domains discretized with unstructured meshes. To this end we consider the reflection of a shock wave from a solid body of triangular shape. The two-dimensional computational domain is the region $[-0.65, 0.5] \times [-0.5, 0.5]$, with a triangular solid body defined by the positions of its vertexes $v_1 = (-0.2, 0), v_2 = (0.1, -1/6)$ and $v_3 = (0.1, 1/6)$. The incident shock wave has shock Mach number $Ms = 1.3$ and at time $t = 0$ is placed at $x = -0.55$, with initial conditions ahead of the shock given by $\rho = 1.225(\text{kg}/\text{ m}^3), p = 1.01325 \times 10^5(\text{Pa})$ and zero velocity. Conditions behind are calculated from the Rankine–Hugoniot conditions.

The mesh consist on 256 580 triangles. Boundary conditions are as follows: left boundary at $x = -0.65$ is defined as inflow condition with the corresponding state defined by the Rankine–Hugoniot conditions; at the right boundary at $x = 0.5$ we set an outflow condition. The remaining boundaries are solid reflecting boundaries.

For the results shown we used the third order ADER scheme along with the Castro–Toro solver for the Derivative Riemann Problem. A CFL coefficient of $C_{cfl} = 0.45$ has been used in the calculations. Figs. 14–17 display Schlieren images for the density at times $t = 7.93 \times 10^{-4}, t = 1.41 \times 10^{-3}, t = 1.85 \times 10^{-3}$ and $t = 2.20 \times 10^{-3}$ respectively. The initial (incident) shock wave propagates to the right, reflects from the triangular solid object generating a circular reflection shock wave. Before the incident shock wave reaches the vertexes v_2 and v_3 of the triangle one can observe the formation of *regular Mach reflection* with well defined Mach stems and slip surfaces on the top and bottom of the triangle. After the incident shock has reached the vertexes v_2 and v_3 two symmetric expansions are created causing a diffraction of the Mach stems and two symmetric vortices. See Fig. 18 for a three dimensional image of the density at time $t = 2.20 \times 10^{-3}$.

The main physical features of the flow resemble those of analogous problems for which there are experimental results, see for example [30].

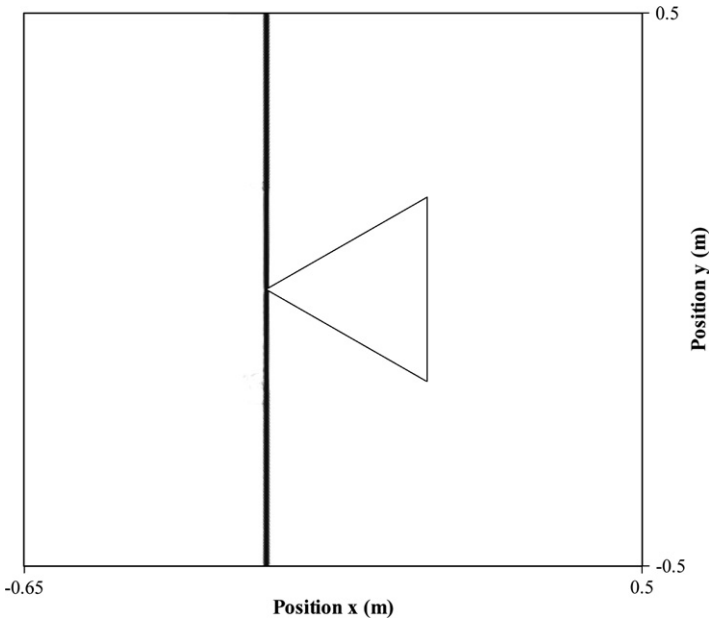

Fig. 14. Shock wave reflection problem. Schlieren image for density at time $t = 7.93 \times 10^{-4}$. Shock wave begins interaction with triangular solid object.

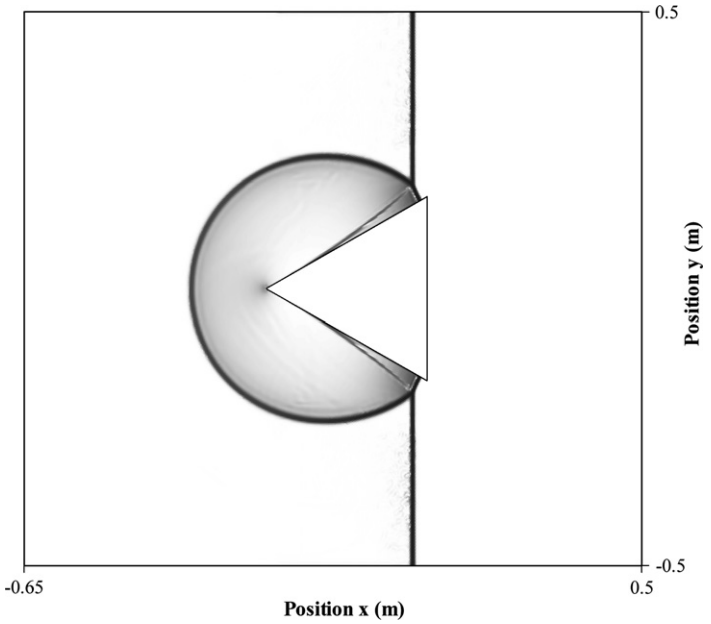

Fig. 15. Shock wave reflection problem. Schlieren image for density at time $t = 1.41 \times 10^{-3}$. Shock wave reflects from edges of triangle and generates regular Mach reflection patterns.

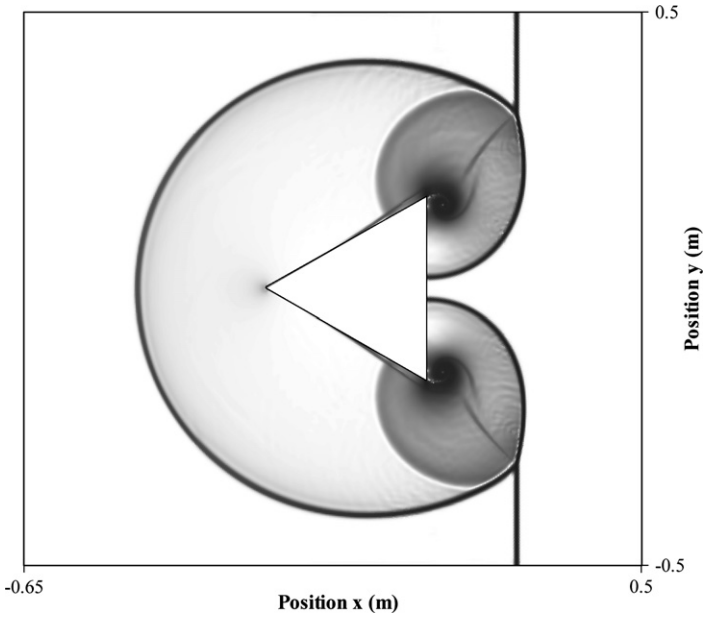

Fig. 16. Shock wave reflection problem. Schlieren image for density at time $t = 1.85 \times 10^{-3}$. Shock wave generates two expansion waves over the corners of the triangle. Slip surfaces are produced from the interaction of the incident shock and the reflected shocks.

6.2. ADER schemes and the well-balanced property

Here we solve the initial-boundary value problem for the one-dimensional shallow water equations with a source term due to bed elevation (77) and (78). We solve the problem using the numerical methods presented in Section 4, for $x \in [-1, 1], t > 0$ with

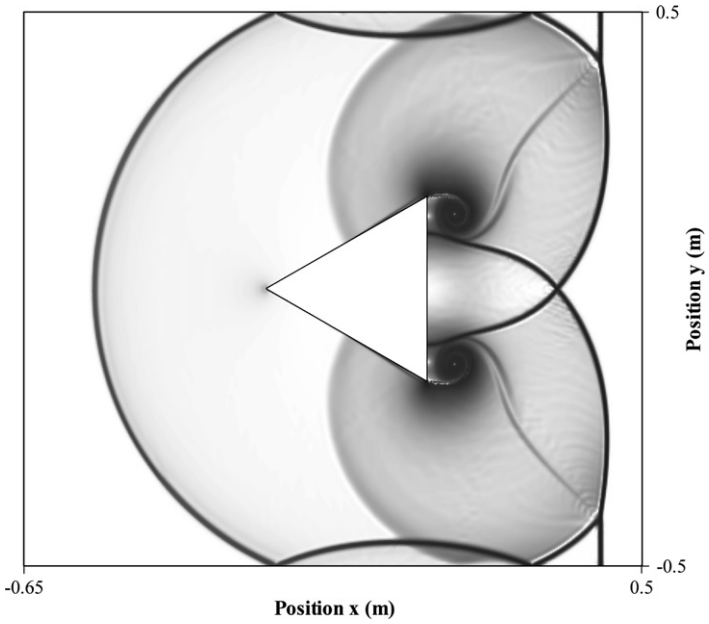

Fig. 17. Shock wave reflection problem. Schlieren image for density at time $t = 2.20 \times 10^{-3}$. Two vortexes evolve behind triangle. Expansion waves interact with shock and with boundaries.

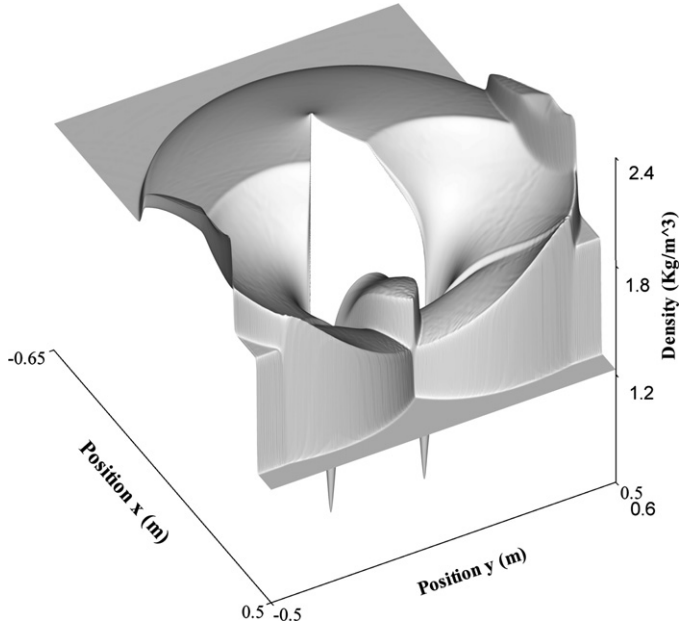

Fig. 18. Shock wave reflection problem. Schlieren image for density at time $t = 2.20 \times 10^{-3}$. Three dimensional image for density.

$$\left.\begin{aligned} &H(x,0) = 1.5,\\ &u(x,0) = 0.0,\\ &b(x) = \tfrac{1}{4}\cos(4\pi x) + \cos(\pi x). \end{aligned}\right\} \tag{88}$$

The exact solution of this particular problem is identical to the initial conditions for all times; that is the free surface remains horizontal and the particle velocity remains zero everywhere for all times. We apply ADER

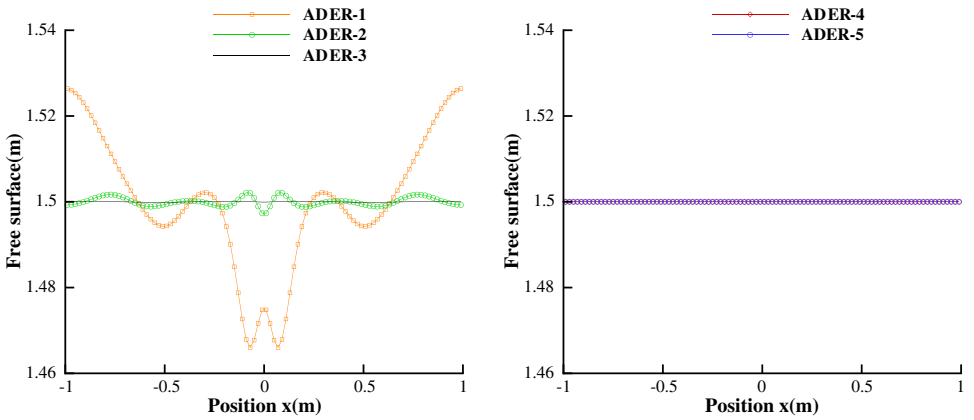

Fig. 19. Shallow water test problem: Comparison of numerical results with the exact solution. Left frame: first to third order ADER schemes. Right frame: fourth and fifth order ADER schemes. Exact solution is $H(x,t) = 1.5$.

Table 9
Shallow water test problem: convergence rates for the fifth order (ADER-5) scheme

Mesh	L_1 error	O_1	L_2 error	O_2	L_∞ error	O_∞
50	9.87×10^{-5}		8.71×10^{-5}		1.49×10^{-4}	
00	3.62×10^{-6}	4.77	3.13×10^{-6}	4.80	5.46×10^{-6}	4.77
200	1.06×10^{-7}	5.09	9.26×10^{-8}	5.08	1.61×10^{-7}	5.09
400	3.43×10^{-9}	4.96	2.96×10^{-9}	4.97	4.89×10^{-9}	5.04
800	1.16×10^{-10}	4.89	9.82×10^{-11}	4.91	1.50×10^{-10}	5.02

finite volume numerical methods of orders one to fifth and evolve the solution for a fixed number 100 of time steps. Numerical results are compared with the exact solution in Fig. 19. The left frame shows the results of the first, second and third order schemes. The right frame of Fig. 19 shows the results for the fourth and fifth order schemes.

The first order scheme (ADER-1) shows a large departure from the exact solution. The second order ADER method (ADER-2) shows a reduced error, while the third order ADER scheme (ADER-3) gives virtually the correct solution. The numerical results of the fourth and fifth order ADER schemes, shown on the right frame of Fig. 19, match very well the correct solution. In summary, as the order of accuracy in the ADER framework is increased one approaches the well-balanced property and one could state that the ADER schemes are asymptotically well-balanced. We remark that neither ad-hoc procedures have been applied, nor particular formulation of the equations have been implemented to obtain the displayed results.

In Table 9 we display the errors of the fifth order ADER solutions for four meshes using three norms. Note that the expected convergence rates are obtained.

7. Summary and concluding remarks

In this paper we have studied three methods for solving the Derivative Riemann Problem for non-linear systems of hyperbolic balance laws. The techniques have been illustrated for the compressible Euler equations of gas dynamics and the shallow water equations with a source term. All three DRP solvers are assessed systematically on a range of *local* derivative Riemann problems. It is found that for linear problems all three solvers are algebraically equivalent, as they are for non-linear systems with smooth initial conditions throughout. For non-linear systems with discontinuous initial conditions the solvers tend to differ amongst themselves, and from the reference solution, as the jump in the initial conditions at the origin increases. For small jumps all solvers tend to give an accurate solution for short times, as one would expect.

We have also implemented the DRP solvers, locally, in the context of high-order finite volume numerical methods of the ADER type. We have applied the numerical methods to solve the Euler equations in two

space dimensions using unstructured meshes; schemes of upto fifth order of accuracy in space and time have been constructed. The empirically obtained convergence rates correspond to the theoretically expected orders of accuracy. An illustration of the potential capabilities of our high-order methods to solve realistic problems on complex domains, using unstructured meshes, has also been given. We have also applied the methods to the nonlinear shallow water equations with a geometric source term due to bed elevation. Through this system we have discussed the so called *well-balanced property* in the context of the ADER schemes. We observe that the ADER schemes may be termed asymptotically well-balanced in that the well-balanced property is attained as the order of accuracy in the ADER schemes is increased, and without any ad-hoc procedures.

Acknowledgments

The authors acknowledge the support provided by the research project PRIN 2004 *Sviluppo di metodi numerici per applicazioni a problemi di fluidodinamica ambientale*, funded by the Italian Ministry of Higher Education and Research.

References

[1] M. Ben-Artzi, J. Falcovitz, A second order Godunov-type scheme for compressible fluid dynamics, J. Comput. Phys. 55 (1984) 1–32.
[2] M. Ben-Artzi, J. Falcovitz, Generalized Riemann Problems in Computational Fluid Dynamics, Cambridge University Press, 2003.
[3] M. Ben-Artzi, J. Li, G. Warnecke, A direct Eulerian GRP scheme for compressible fluid flows, J. Comput. Phys. 218 (2006) 19–43.
[4] M. Ben-Artzi, J. Li, Hyperbolic balance laws: Riemann invariants and hyperbolic balance laws, Numerische Mathematik 106 (2007) 369–425.
[5] A. Bourgeade, P. LeFloch, P.A. Raviart, An Asymptotic expansion for the solution of the generalized Riemann problem. Part 2: Application to the Euler equations of gas dynamics, Ann. Inst. Henri Poincaré. Analyse non Lineáre 6 (6) (1989) 437–480.
[6] P. Colella, A direct Eulerian MUSCL scheme for gas dynamics, SIAM J. Sci. Stat. Comput. 6 (1985) 104–117.
[7] M. Dumbser, Arbitrary high order schemes for the solution of hyperbolic conservation laws in complex domains. PhD thesis, Institut für Aero- un Gasdynamik, Universität Stuttgart, Germany, 2005.
[8] M. Dumbser, M. Käser, Arbitrary high order non-oscillatory finite volume schemes on unstructured meshes for linear hyperbolic systems, J. Comput. Phys. 221 (2007) 693–723.
[9] M. Dumbser, C.D. Munz, ADER discontinuous Galerkin schemes for aeroacoustics, Comptes Rendus Mécanique 333 (2005) 683–687.
[10] M. Dumbser, T. Schwartzkopff, C.D. Munz, Arbitrary high order finite volume schemes for linear wave propagation, Computational Science and High Performance Computing II: Notes on Numerical Fluid Mechanics and Multidisciplinary Design, vol. 91, Springer, 2006, 129–144.
[11] M. Dumbser, M. Käser, V.A. Titarev, E.F. Toro, Quadrature-free non-oscillatory finite volume schemes on unstructured meshes for nonlinear hyperbolic systems, J. Comput. Phys. 226 (2007) 204–243.
[12] S.K. Fok, Extension of Glimm's method to the problem of gas flow in a duct of variable cross-section. PhD Thesis, Department of Mathematics, University of California, Berkeley, 1981.
[13] J. Glimm, Solution in the large for nonlinear hyperbolic systems of equations, Commun. Pure Appl. Math. 18 (1965) 697–715.
[14] J. Glimm, G. Marshall, B. Plohr, A generalized Riemann problem for quasi one-dimensional gas flows, Advances in Applied Mathematics 5 (1984) 1–30.
[15] S.K. Godunov, Finite difference methods for the computation of discontinuous solutions of the equations of fluid dynamics, Mat. Sb. 47 (1959) 271–306.
[16] E. Harabetian, A convergent series expansion for hyperbolic systems of conservation laws, Trans Am. Math. Soc. 294 (1986) 383–424.
[17] A. Harten, B. Engquist, S. Osher, S.R. Chakravarthy, Uniformly high order accuracy essentially non-oscillatory schemes III, J. Comput. Phys. 71 (1987) 231–303.
[18] A. Harten, S. Osher, Uniformly high–order accurate nonoscillatory schemes I, SIAM J. Numer. Anal. 24 (2) (1987) 279–309.
[19] C. Hu, C.W. Shu, Weighted essentially non-oscillatory schemes on triangular meshes, J. Comput. Phys. 150 (1999) 97–127.
[20] G.S. Jiang, C.W. Shu, Efficient implementation of weighted ENO schemes, J. Comput. Phys. 126 (130) (1996) 202–228.
[21] M. Käser, Adaptive Methods for the Numerical Simulation of Transport Processes. PhD thesis, Institute of Numerical Mathematics and Scientific Computing, University of Munich, Germany, 2003.
[22] M. Käser, A. Iske, ADER Schemes for the solution of conservation laws on adaptive triangulations, Mathematical Methods and Modelling in Hydrocarbon Exploration and Production. Mathematics in Industry, vol. 7, Springer-Verlag, 2005, pp. 323–385.
[23] M. Käser, A. Iske, Adaptive ADER schemes for the solution of scalar non-linear hyperbolic problems, J. Comput. Phys. 205 (2005) 486–508.
[24] L. Tatsien, Y. Wenci. Boundary-value problems for quasi-linear hyperbolic systems, Duke University Mathematics Series, 1985.
[25] P. Le Floch, P.A. Raviart, An asymptotic expansion for the solution of the generalized riemann problem. Part 1: General theory, Ann. Inst. Henri Poincaré. Analyse non Lineáre 5 (2) (1988) 179–207.

[26] P. Le Floch, L. Tatsien, A global asymptotic expansion for the solution of the generalized riemann problem, Ann. Inst. Henri Poincaré. Analyse non Lineáre 3 (1991) 321–340.
[27] T.P. Liu, Quasilinear hyperbolic systems, Commun. Math. Phys. 68 (1979) 141–172.
[28] I.S. Men'shov, Increasing the order of approximation of Godunov's scheme using the generalized Riemann problem, USSR Comput. Math. Phys. 30 (5) (1990) 54–65.
[29] V.P. Kolgan, Application of the principle of minimum derivatives to the construction of difference schemes for computing discontinuous solutions of Gas dynamics (in Russian), Uch. Zap. TsaGI, Russia 3 (6) (1972) 68–77.
[30] H. Schardin, in: Proceedings of VII International Congress on High Speed Photg. Darmstadt, O. Helwich Verlag, 1965.
[31] T. Schwartzkopff, Finite-Volumen Verfahren hoher Ordnung und heterogene Gebietszerlegung ü die numerische Aeroakustik. PhD thesis, Institut für Aero- un Gasdynamik, Universität Stuttgart, Germany, 2005.
[32] T. Schwartzkopff, C.D. Munz, E.F. Toro, ADER: high-order approach for linear hyperbolic systems in 2D, J. Sci.Comput. 17 (2002) 231–240.
[33] T. Schwartzkopff, M. Dumbser, C.D. Munz, Fast high-order ADER schemes or linear hyperbolic equations, J. Comput. Phys. 197 (2004) 532–539.
[34] C.W. Shu, S. Osher, Efficient implementation of essentially non-oscillatory shock-capturing schemes II, J. Comput. Phys. 83 (1988) 32–78.
[35] C.W. Shu, S. Osher, Efficient implementation of essentially non-oscillatory shock-capturing schemes, J. Comput. Phys. 77 (1988) 439–471.
[36] Y. Takakura, E.F. Toro, Arbitrarily accurate non-oscillatory schemes for a non-linear conservation law, J. Comput. Fluid Dyn. 11 (1) (2002) 7–18.
[37] V.A. Titarev, E.F. Toro, ADER: arbitrary high order Godunov approach, J. Sci. Comput. 17 (2002) 609–618.
[38] V.A. Titarev, E.F. Toro, ADER schemes for three-dimensional hyperbolic systems, J. Comput. Phys. 204 (2005) 715–736.
[39] E.F. Toro, Riemann Solvers and Numerical Methods for Fluid Dynamics, Springer–Verlag, 1997.
[40] E.F. Toro, Primitive, conservative and adaptive schemes for hyperbolic conservation laws, in: E.F. Toro, J.F. Clarke (Eds.), Numerical Methods for Wave Propagation, Kluwer Academic Publishers, 1998, pp. 323–385.
[41] E.F. Toro, Riemann Solvers and Numerical Methods for Fluid Dynamics, second ed., Springer-Verlag, 1999.
[42] E.F. Toro, R.C. Millington, L.A.M. Nejad, Towards very high-order Godunov schemes, in: E.F. Toro (Ed.), Godunov Methods: Theory and Applications, Kluwer Academic/Plenum Publishers, 2001, pp. 905–937 (Edited Review).
[43] E.F. Toro, Shock-Capturing Methods for Free-Surface Shallow Flows, Wiley and Sons Ltd., 2001.
[44] E.F. Toro, V.A. Titarev, Solution of the generalised Riemann problem for advection-reaction equations, Proc. Roy. Soc. London A 458 (2002) 271–281.
[45] E.F. Toro, V.A. Titarev, ADER schemes for scalar hyperbolic conservation laws with source terms in three space dimensions, J. Comput. Phys. 202 (1) (2005) 196–215.
[46] E.F. Toro, V.A. Titarev, Derivative Riemann solvers for systems of conservation laws and ADER methods, J. Comput Phys. 212 (1) (2006) 150–165.
[47] B. van Leer, Towards the ultimate conservative difference Scheme I. The quest for monotonicity, Lecture Notes in Physics 18 (1973) 163–168.
[48] B. van Leer, On the relationship between the upwind-differencing schemes of Godunov, Engquist–Osher and Roe, SIAM J. Sci. Stat. Comput. 5 (1) (1985) 1–20.